Climate Dynamics (2021) 57:1039–1060
https://doi.org/10.1007/s00382-021-05757-1

Linking the Madden–Julian Oscillation, tropical cyclones and westerly wind bursts as part of El Niño development

Yu Liang[1] · **Alexey V. Fedorov**[1,2]

Received: 4 April 2020 / Accepted: 30 March 2021 / Published online: 15 April 2021

Abstract
Westerly wind bursts (WWBs) that occur over the western and central equatorial Pacific are believed to play an important role in ENSO dynamics; however, the mechanisms of WWB generation are still debated. In this study we investigate a link between the Madden–Julian Oscillation (MJO) and WWBs that involves tropical cyclones (TCs) generated within the MJO sufficiently close to the equator. Using an atmospheric reanalysis and WWB composites, we first isolate WWBs that occur (1) between December and April and (2) between May and November, corresponding to the onset and development stages of El Niño. We find that during the onset stage, a warm background sea surface temperature (SST) anomaly develops over the central-western equatorial Pacific with anomalous westerly winds to its west, which draws the MJO convective activity in the southern hemisphere closer to the equator. As a result, westerly wind anomalies associated with the MJO together with tropical cyclones embedded in the MJO induce strong WWBs (during neutral conditions the MJO usually takes a more southerly route and cannot induce strong bursts). Subsequently, during the development stage of El Niño, there develops an anomalous warming in the central-eastern equatorial Pacific, also with corresponding westerly winds, which steers the MJO path, now in the northern hemisphere, toward the equator, strengthening the MJO signal over the central equatorial Pacific. Consequently, tropical cyclones modulated by the MJO move closer to the equator and farther east, facilitating WWBs. Thus, MJO events with embedded tropical cyclones are crucial for the generation process of WWBs during the onset and development of El Niño.

Keywords El Niño · Westerly wind bursts · Madden-Julian oscillation · Tropical cyclones

1 Introduction

The El Niño–Southern Oscillation (ENSO) is the most important interannual climate mode of the ocean–atmosphere system with far-reaching impacts on global climate, ecosystems, fisheries and human activities (e.g., McPhaden et al. 2006a; Timmermann et al. 2018). However, despite great advances in understanding El Niño dynamics and its global impacts during the past several decades (e.g., Guilyardi et al. 2009, 2012; Capotondi et al. 2015; McPhaden et al. 2020), it is still difficult to predict the development of El Niño accurately, which is in part due to our inability to forecast the occurrence and impacts of episodic atmospheric disturbances in the tropical Pacific that appear in the form of equatorial westerly wind bursts (WWBs) (e.g., Harrison and Vecchi 1997; McPhaden 1999; Fedorov 2002; Lengaigne et al. 2002; Fedorov et al. 2003; McPhaden 2004; Eisenman and Tziperman 2005; Fedorov et al. 2015; Hu and Fedorov 2017; Hu et al. 2014; Puy et al. 2016; Yu and Fedorov 2020).

WWBs induce strong westerly wind anomalies in the western and central equatorial Pacific, often observed at the onset and development stages of El Niño (Fedorov 2002; McPhaden 2004; Seiki and Takayabu 2007a; Chen et al. 2015; Timmermann et al. 2018). They usually last for several days to weeks (Fig. 1), have a zonal extent of more than 10° of longitude, meridional width of 10°–15° of latitude and wind speed anomalies of 5–7 m/s (Harrison and Vecchi 1997; Puy et al. 2016), up to ~ 10 m/s as seen in the present study. WWBs can induce eastward advection of warm surface waters, warming the central equatorial Pacific, and at the same time induce eastward

✉ Yu Liang
yu.liang@yale.edu

[1] Department of Earth and Planetary Sciences, Yale University, New Haven, Connecticut, USA

[2] LOCEAN/IPSL, Sorbonne University, Paris, France

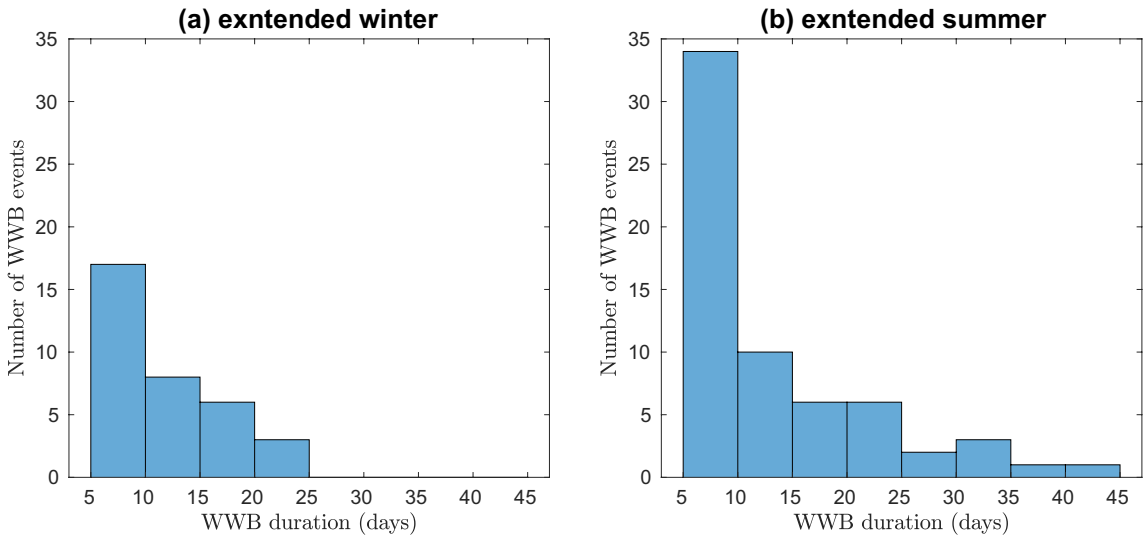

Fig. 1 Histograms showing the distribution of WWB duration for wind bursts generated in **a** the extended winter season (DJFMA) and **b** the extended summer season (MJJASON). The average duration is 11 days in **a** and 13 days in **b**. Note that two WWBs whose duration formally exceeds 45 days were split into several shorter bursts driven by different processes. Also note that for these and all other estimates shown throughout the paper, El Niño decay periods are excluded, and the years of calculations are 1979–2016

propagating Kelvin waves, depressing the thermocline and warming the eastern equatorial Pacific (e.g., McPhaden 1999; McPhaden and Yu 1999; Vecchi and Harrison 2000; Fedorov 2002; Lengaigne et al. 2002; Hu et al. 2014; Hu and Fedorov 2017). Recent studies also show that adding WWBs can make simulated El Niño events more realistic (Gebbie et al. 2007; Levine et al. 2016) and contribute to the diversity of El Niño events (e.g., Hu et al. 2014; Fedorov et al. 2015; Chen et al. 2015; Thual et al. 2016). They also contribute to ENSO irregularity and decadal modulation (e.g., Yu and Fedorov 2020; Fedorov et al. 2020; An et al. 2020 and references therein).

Given the importance of WWBs in El Niño dynamics and prediction, the causes of WWBs have been investigated in a number of studies. In simple models, WWBs are often treated as stochastic forcing (Battisti and Hirst 1989; Neelin and Jin 1993; Fedorov et al. 2003). However, they typically occur more frequently during El Niño years and migrate eastwards with the development of El Niño (Harrison and Vecchi 1997; Eisenman et al. 2005; Seiki and Takayabu 2007a). About half of the variance of WWBs is explained by two large-scale sea surface temperature (SST) modes (Tziperman and Yu 2007), and the characteristics of WWBs can be represented as a linear function of SST (Gebbie and Tziperman 2009). Therefore, WWBs can be state-dependent and a number of models represent them as multiplicative rather than additive noise (e.g., Levin et al. 2016; Levine and Jin 2017; Thual et al. 2016).

Various weather systems have been proposed as potential causes of WWBs, including cold surges (Chu 1988), convectively coupled Rossby waves (Puy et al. 2016), tropical cyclones (Hartten 1996; Seiki and Takayabu 2007b; Lian et al. 2018) and the Madden–Julian Oscillation (McPhaden 1999; Seiki and Takayabu 2007a; Puy et al. 2016; Feng and Lian 2018), of which the Madden–Julian Oscillation (MJO) has been thought as perhaps the most important because it can generate spatially and temporally coherent WWBs.

The MJO is the dominant intra-seasonal mode of variability in the tropical atmosphere with zonal wavenumbers 1–5 and a period of 30–95 days, providing a convective envelope for different coupled atmospheric systems (Wheeler and Kiladis 1999; Zhang 2005). WWBs are usually found during the convective MJO phase (McPhaden 1999; Seiki and Takayabu 2007a; Puy et al. 2016; Lian et al. 2018) when large-scale westerly wind anomalies develop to the west of the convective center (Zhang 2005). Seiki and Takayabu (2007a) suggested that stronger MJO events tend to bear more WWBs; Puy et al. (2016) found that nearly 60% WWBs are associated with westerly winds within the MJO, even though this number and other similar estimates are typically quite sensitive to the chosen definition of WWBs.

Because of the importance of the MJO in El Niño dynamics, many studies explored the relationship between the two phenomena. The globally integrated MJO activity is found to be weakly correlated with ENSO, suggesting that interannual variations in the MJO activity are mostly internally generated (Slingo et al. 1999; Hendon et al. 1999). However, enhanced MJO activity has been observed over the western equatorial Pacific during boreal spring preceding El Niño, which is hypothesized to favor El Niño development (McPhaden et al. 2006b; Hendon et al. 2007). An eastward extension of the MJO convective envelope has

been also observed during El Niño development (Kessler 2001; Hendon et al. 1999). However, most of these studies, as pointed out by Roundy and Kravitz (2009), only examine correlations between various indices of the MJO (usually represented by equatorially averaged outgoing long wave radiation, OLR, or zonal wind anomalies) and the indices of ENSO, but neglect for example to study variations in the MJO horizontal structure that may be important for ENSO. As revealed by the present study, changes in the MJO horizontal structure are indeed one of the main causes of the enhanced MJO activity in the equatorial band and WWB generation in El Niño years.

The MJO also modulates the genesis and propagation of tropical cyclones (TCs) as TCs preferentially occur in the convective phase of the MJO (e.g., Liebman et al. 1994; Sobel and Maloney 2000; Camargo et al. 2009). Tropical cyclones have also been suggested to generate WWBs (e.g., Harrison and Giese 1991; Hartten 1996; Harrison and Vecchi 1997), and some of the observed TCs appear within the westerly phase of the MJO (e.g., Lian et al. 2018). During El Niño years, the zonal displacement of cyclogenesis locations in the western North Pacific (e.g., Lander 1994; Sobel and Maloney 2000) and their equatorward shift in the South Pacific (e.g., Revell and Goulter 1986; Hastings 1990; Vincent et al. 2011) have been also observed. The equatorward shift of TC activity has been mentioned in the context of WWB generation (Seiki et al. 2007b; Lian et al. 2018).

Despite the presumed general relationship between WWBs, the MJO and TCs, possibly modulated by SST, several key issues of WWB generation have not been adequately addressed by prior studies. In particular, how do changes in the MJO horizontal structure influence WWB generation during the onset and development stages of El Niño (as typical westerly winds associated with the MJO are too weak on the equator)? What is the role of tropical cyclones embedded in the MJO in WWB generation? Since WWBs can act as multiplicative noises, can we quantify the dependence of WWB intensity on tropical Pacific SST during different seasons?

Furthermore, many previous studies investigated the statistical relationship between the MJO and WWBs without considering its seasonality (Seiki and Takayabu 2007a; Puy et al. 2016), even though the MJO varies seasonally—it is more active in the southern hemisphere during boreal winter and in the northern hemisphere during boreal summer (Wheeler and Hendon 2004). In addition, with the development of El Niño the dominant location of WWBs shifts eastward between spring and summer—during the onset stage of El Niño (boreal winter and spring, from December to April), WWBs usually occur over the western equatorial Pacific, while during the development stage of El Niño (late boreal spring, summer and fall, from May to November) they are observed over the central equatorial Pacific (Seiki and Takayabu 2007a).

Accordingly, the goal of the present study is to describe robust links between WWBs, the MJO, TCs, and tropical Pacific SST anomalies during different stages of El Niño evolution. Using atmospheric reanalysis data, we will first identify WWBs and separate them into two groups—(1) those that occur from December to April, and (2) those that occur from May to November. These two periods broadly correspond to the onset and development stages of El Niño, respectively. Note that in this study the decay stage of El Niño is excluded, as we focus on WWBs that contribute to the initiation and development of El Niño events (see further details in Sect. 2.3). We will then investigate the underlying (background) SST and wind anomalies preceding WWBs, and the relevant characteristics of the MJO during the process of wind burst generation. As the MJO is known to modulate TC genesis (Liebmann et al. 1994), we will analyze the tracks of TCs embedded in the active phase of the MJO to provide a unified picture of how tropical Pacific SST anomalies affect WWB generation via the MJO and MJO-embedded TCs during the onset and development stages of El Niño.

The rest of this paper is organized as follows: Datasets and methods used to define El Niño events, WWBs, the MJO and TCs are described in Sect. 2. The composite analysis of data is presented in Sect. 3, which is followed by our conclusions and discussion (Sect. 4). A complementary paper explores these ideas using simulations with an atmospheric GCM (Liang et al. 2020).

2 Datasets and methods

2.1 Datasets

We use daily zonal and meridional wind speeds at 1000 hPa and the SST field with a horizontal resolution of 1° from the ERA-interim dataset which spans from Jan 1979 to Dec 2016 (Dee et al. 2011). The NOAA interpolated daily outgoing longwave radiation (OLR) with a horizontal resolution of 2.5° is also used with the same temporal coverage (Liebmann and Smith 1996). To define El Niño events, we apply the Oceanic Niño Index (ONI), which is given by a 3-month running mean of SST anomalies in the Niño 3.4 region (5°N–5°S, 120°–170°W) based on the ERSST.v5 dataset (Huang et al. 2017). Anomalies are relative to centered 30-year base periods updated every 5 years as described in https://origin.cpc.ncep.noaa.gov/products/analysis_monitoring/ensostuff/ONI_v5.php. TC tracks in the western North Pacific, East Pacific and South Pacific with a 6-hourly time step are from the International

Best Track Archive for Climate Stewardship (IBTrACS v04), which also spans from Jan 1979 to Dec 2016 (https://www.ncdc.noaa.gov/ibtracs/).

2.2 Definition of El Niño events

The ONI is used to define El Niño events and their duration. If the ONI remains larger than 0.5 °C for a minimum of 5 consecutive months, an El Niño event is said to occur. El Niño is typically phase locked to the seasonal cycle (e.g., Rasmusson and Carpenter 1982; Hirst 1986; Iskandar et al. 2018)—events start in boreal winter and early spring (December–April), develop in late spring, summer and fall (May–November), peak in December and decay in the following spring, even though there are some variations around this canonic development (e.g., Neelin et al. 2000; Wu et al. 2019). For our analysis, the year when El Niño develops and peaks is called year (0); the years before and after are called year (−1) and year (+1), respectively.

The interval from December of year (−1) to April of year (0) is defined as the onset stage of El Niño, during which the ONI is usually smaller than 0.5 °C and there usually occurs the first sequence of WWBs in the western equatorial Pacific. April is chosen as the last month of the onset stage because of the well-known spring predictability barrier of El Niño (Torrence and Webster 1998; McPhaden 2003). We refer to this winter-spring period as the extended winter season.

The interval from May to November in year (0) is defined as the development stage of El Niño, when WWBs over the equatorial central Pacific act to maintain and further enhance warm SST anomalies (Vecchi and Harrison 2000; Hu and Fedorov 2016, 2017). We refer to this late-spring–summer-fall period as the extended summer season.

The decay stage of El Niño is defined as December in year (0) until the final month in year (+1) as long as the ONI stays above 0.5 °C. We exclude this decay stage of El Niño when computing various estimates and composites as we focus on WWBs that contribute to the initiation and development of El Niño events.

Two prolonged El Niño events in the studied period persisted and reached their second peak in year (+1). One was in 1986–1988 and the other was in 2014–2016. Therefore, for analyzing WWBs we treat the intervals from May to November in 1987 and 2015 as the development stage of El Niño events, but exclude the intervals from December 1986 to April 1987 and December 2014 to April 2015 from the onset stage of El Niño, although the results would not change if these two time intervals were included.

2.3 Definition of westerly wind bursts

There are several ways to define WWBs. Here, they are defined by considering zonal wind speed anomalies at 1000 hPa (U1000hPa), rather than surface wind stress for example. We firstly compute a 5-day running-mean daily climatological U1000hPa during 1979–2016, and then calculate daily wind anomalies relative to this climatology. This method is similar to the study of Seiki and Takayabu (2007a), except that they used a much smoother, 91-day running-mean daily climatology. In contrast, to identify WWBs Puy et al. (2016) applied a 5–90 days band-pass filtering to wind stress, but such an approach sometimes weakens strong and persistent westerly bursts but introduces artificial easterly bursts. Because strong WWBs are especially important in initiating and maintaining the development of El Niño, in our study we define westerly wind anomalies relative to the 5-day running-mean daily climatology.

When identifying WWBs we use four criteria: (1) U1000hPa anomalies averaged between 3°N and 3°S are stronger than the 5 m/s threshold. (2) The area that satisfies the wind speed criterion has a zonal extent of at least 10° of longitude. (3) The first two criteria are met for at least 5 days. The latitudinal extent is chosen as approximately one oceanic (baroclinic) Rossby radius of deformation at the equator, because only westerly wind anomalies within this meridional band can excite oceanic Kelvin waves effectively (Fedorov and Brown 2009). (4) In addition, if two wind anomalies are separated by less than 3° of longitude and 3 days, they are considered as one WWB.

When considering the extreme El Niño events of 1982 and 1997, an additional treatment of WWBs is needed since during these events there developed very strong westerly wind anomalies in response to the warming in the eastern equatorial Pacific as part of the ENSO cycle (e.g., McPhaden 1999; Lengaigne and Vecchi 2010; Zhao and Fedorov 2020). These inter-seasonal westerly anomalies connect separate WWB events and create the appearance of "super bursts" lasting for about four months (Figs. S1 and S2), which exceeds the normal duration of WWBs (several days to weeks). Thus, to maintain consistency among the characteristics and physical mechanisms of different wind bursts, in this study we split WWBs that lasted for more than 45 days into shorter bursts generated by different processes. The 45 days threshold is chosen as it corresponds to the longest half period of intraseasonal anomalies typically associated with the MJO. For example, we separate a WWB generated during the westerly phase of the MJO from the subsequent WWB generated during the easterly phase of the MJO in 1982 (see discussion in Sect. 2.4). While this separation is not necessarily unique, it does not affect the main results of this study. For the extreme

El Niño event of 2015, WWBs are relatively well separated (i.e., no WWBs exceeded 45 days).

In total, 125 WWBs are identified from 1979 to 2016 with 3.3 events per year on average. This number is smaller than 8 events per year reported in Seiki and Takayabu (2007a) because they used less strict criteria for WWB identification (e.g., minimum duration of 2 days, and some of seasonal variations were included in wind bursts).

Because of seasonal variations in WWBs during El Niño evolution, we separate the observed wind bursts into two groups in accordance with the time of their generation. Group 1 is from December to April (DJFMA, the extended winter season) and group 2 is from May to November (MJJASON, the extended summer season), which correspond to the onset and development stages of El Niño, respectively. Note that nearly all WWB events in 1979–2016 are studied, including those during non-El Niño periods, except for WWBs during the decay stage of El Niño, as our focus is on the onset and development of El Niño. For example, in January of 1998, two WWBs occurred, but they are excluded from Group 1. Even though those excluded WWBs may play a role in extending the El Niño duration, they do not contribute to the event growth. After removing those WWB events, 97 qualified WWB events remain. The statistical distribution of their duration in the extended winter and summer seasons is shown in Fig. 1.

To measure the strength of a WWB, we first integrate zonal wind anomalies averaged between 3°N and 3°S over longitude for each day during the event using Eq. (1) below to obtain ano_{day}, and then integrate ano_{day} over the duration of the event using Eq. (2) to obtain Amp_{wwb}. The central date day_0 of each WWB is defined by a weighted average in Eq. (3), where *day(t)* denotes time (date) within the WWB considered. Similarly, we compute the central longitude lon_0 of WWB on day_0 using Eq. (4) and *lon(x)* denotes longitude within the region where zonal wind anomalies of the WWB are observed. This definition assures that $U1000hPa_{ano}$ at the center of WWBs reaches the 5 m/s threshold. Examples of WWBs for the year 2015 are shown in the Hovmoller diagram in Fig. 2a in which yellow patches circled by red contours represent averaged U1000hPa anomalies that exceed 5 m/s. If all criteria of WWB are met, a filled red circle centered at day_0 and lon_0 with a radius proportional to Amp_{wwb} is plotted in Fig. 2b, c to represent the WWB.

$$ano_{day} = \int_{lon} U1000hPa_{ano}(x, day)dx, \tag{1}$$

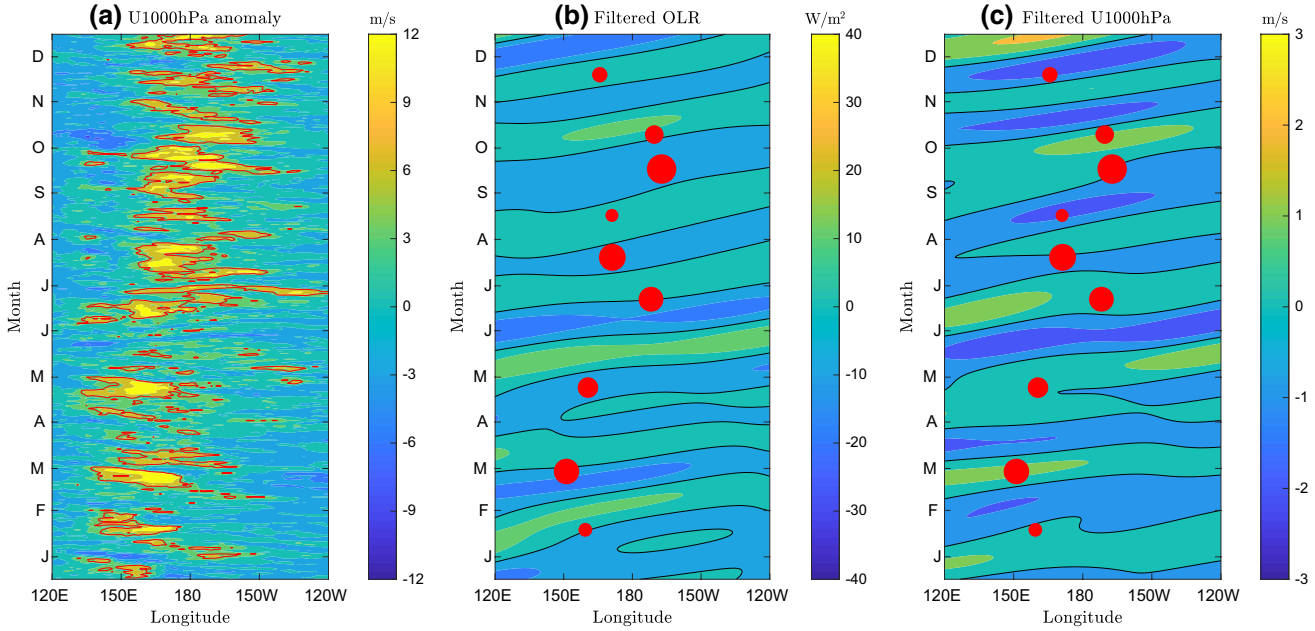

Fig. 2 Example of WWBs and MJO events in the year 2015. **a** U1000hPa anomalies averaged between 3°N and 3°S (color shading; shading interval of 3 m/s). Wind anomalies are calculated relative to the daily climatology with a 5-day running-mean applied. Red contours indicate the 5 m/s threshold. **b** Space–time filtered OLR variations averaged between 15°N–15°S with the color shading interval of 10 W/m^2. The band-pass filtering retains zonal wavenumbers 1–5 and periods between 30–95 days. Black contours indicate zero values. Negative (positive) values represent the MJO convective (suppressed) phase. **c** Space–time filtered U1000hPa variations averaged between 15°N–15°S with the color shading interval of 1 m/s. Black contours indicate zero values. Negative (positive) values represent the MJO easterly (westerly) phase. Solid red circles in **b** and **c** mark WWB events; the circle radius is proportional to the strength of the bursts (Amp_{wwb}). Note the differences between wind variations as presented in **a** and **c**

$$Amp_{wwb} = \int_{lon}\int_{t} U1000hPa_{ano}(x,t)dxdt, \quad (2)$$

$$day_0 = \frac{\int_{lon}\int_{t} U1000hPa_{ano}(x,t)day(t)dxdt}{Amp_{wwb}}, \quad (3)$$

$$lon_0 = \frac{\int_{lon} U1000hPa_{ano}(x,day_0)lon(x)dx}{ano_{day_0}}. \quad (4)$$

2.4 Definition of MJO events

The space–time filtering is used to isolate the MJO signal. Zonal and meridional wind velocities at 1000 hPa and outgoing longwave radiation (OLR) are filtered to retain only eastward propagating signals with zonal wave numbers 1–5 and periods of 30–95 days (following Wheeler and Kiladis 1999). Negative (positive) OLR anomalies correspond to the convective (suppressed) phase of the MJO; westerly (easterly) wind anomalies correspond to the westerly (easterly) phase of the MJO. As an example, we show the filtered OLR and U1000hPa fields for the year 2015 (averaged between 15°N and 15°S, Fig. 2b, c). Both OLR and wind anomalies propagate eastwards at a speed of about 5 m/s, with negative OLR anomalies usually leading westerly wind anomalies by a few days (Madden and Julian 1972; Rui and Wang 1990; Zhang 2005; Seiki and Takayabu 2007b).

Using the criterion that negative OLR anomalies averaged over the western Pacific (120°E–180°, 15°N–15°S) should exceed 0.8 times standard deviation for at least 10 days, we identify 146 MJO events in 1979–2016, with 3.7 MJO events each year on average. Note that we use the 0.8 times standard deviation threshold because the summer MJO is generally weaker than the winter MJO. Even with this threshold the maximum averaged OLR anomalies for each MJO event still exceed one standard deviation. The amplitude of the MJO (Amp_{MJO}) is computed as the absolute value of the largest negative OLR anomaly averaged over the western Pacific (120°E–180°, 15°N–15°S).

The date when average westerly wind anomalies of the MJO in this region reach maximum is denoted as $day_{westerly}$ (note the difference from day_0 for WWBs). We find that on average $day_{westerly}$ leads day_0 1 day in the extended winter season and 3 days in the extended summer season (Fig. S3), in agreement with Seiki and Takayabu (2007a). Finally, we divide MJO events into two groups in terms of their relationship to WWBs: If the central date (day_0) of a WWB event occurs in the westerly phase of an MJO, the MJO is referred to as a WWB-generating MJO (wMJO); otherwise, it is a nonWWB-generating MJO (nwMJO). None of WWBs analyzed in this study spans two MJO events.

3 Composite analysis

3.1 WWBs in the extended winter season

We first investigate how the MJO with embedded TCs generates WWBs during the extended winter season (DJFMA, with El Niño decay periods excluded). During the time interval we consider (years 1979–2016), 23 wMJO and 34 nwMJO events in total are identified. Since typically only strong MJO events can generate WWBs (Seiki and Takayabu 2007a; Hendon et al. 2007; Puy et al. 2016; Liang et al. 2020), top 34 strongest MJO events are selected during this period in accordance with Amp_{MJO}, among which 16 are wMJO events and 18 are nwMJO events. The following analysis would give very similar results if all MJO events during this period were considered.

To assess differences between these wMJO and nwMJO events, in Fig. 3 we compare their composites for OLR (panels b, d) and surface wind anomalies (panels a, c) on $day_{westerly}$. The wMJO and nwMJO have a generally similar spatial structure. The centers of convective and westerly wind anomalies are both located in the southern hemisphere with negative OLR anomalies leading westerly wind anomalies by 10–15 degrees of longitude. On average, the wMJO events are stronger than the nwMJO events in terms of their OLR anomalies, which is consistent with the idea that strong MJO events tend to generate WWBs (Seiki and Takayabu 2007a).

Additionally, several other significant differences between the wMJO and nwMJO are found: (1) Negative OLR anomalies of the nwMJO in the southern hemisphere have a northwest-southeast alignment corresponding to the structure of the South Pacific convergence zone (SPCZ), while convective activity in the northern hemisphere remains much weaker than in the southern hemisphere (panel d). However, for the wMJO (panel b), negative OLR anomalies are nearly parallel to the equator, suggesting stronger convective activity near the equator. Even though convection remains relatively weak in the northern hemisphere, it still strengthens relative to the nwMJO (panel f). (2) Similar to the differences in OLR anomalies, there occurs a shift in the structure of westerly wind anomalies toward the equator in the southern hemisphere during the wMJO compared to the nwMJO (panels a, c, e). As westerly wind anomalies can only effectively excite Kelvin waves within several degrees north and south of the equator, this change in wind structure is important for WWB generation.

To explore what causes these differences, we next compute the difference between the wMJO and nwMJO composites of background SST and zonal surface winds (Fig. 4). The wMJO and nwMJO composites of background SST and zonal surface winds are also shown in Fig. S4 for reference.

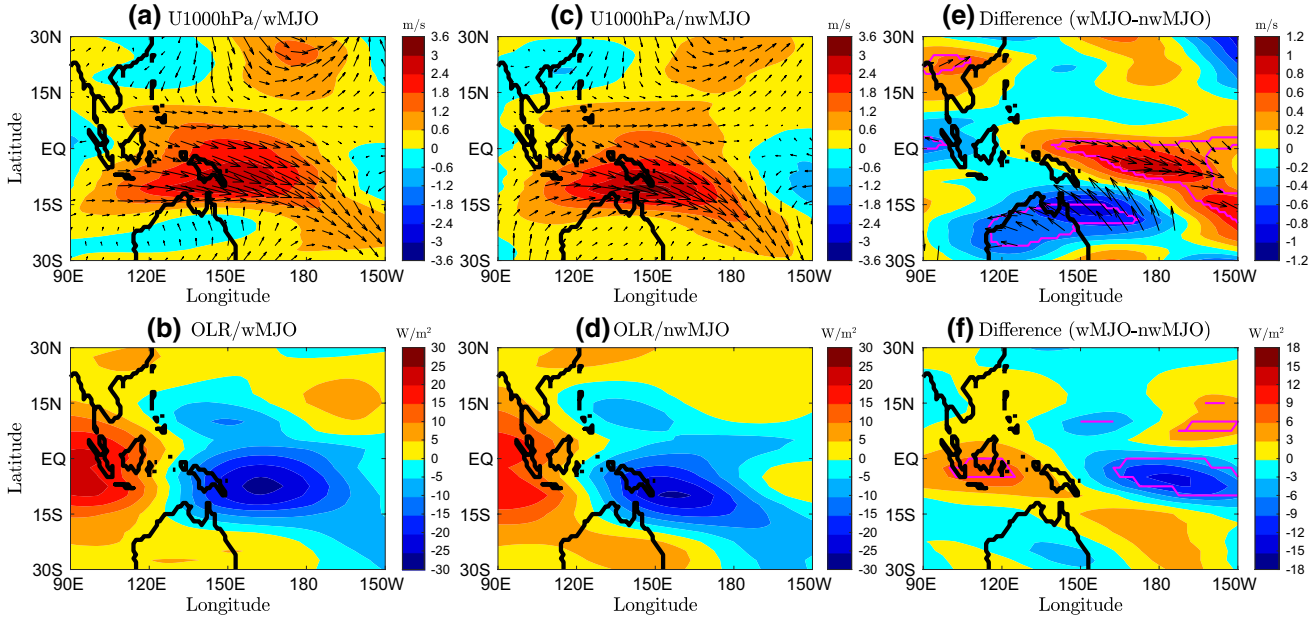

Fig. 3 Extended winter season (DJFMA) composites of **a** filtered 1000 hPa wind speed anomalies on $day_{westerly}$ and **b** filtered OLR anomalies also on $day_{westerly}$ for 16 wMJO events selected during 1979–2016. **c** and **d** Display the same variables but for 18 nwMJO events. **e** and **f** Show the difference between the wMJO and nwMJO composites (i.e., left column minus middle column). Band-pass space–time filtering is used to isolate the MJO signal (zonal wavenumbers 1–5, periods between 30–95 days). In the top row: black arrows indicate filtered wind anomalies and color shading denotes U1000hPa anomalies; in the bottom row: color shading denotes OLR anomalies. The intervals of color shading are 0.6 m/s in **a**, **c**, and 0.2 m/s in **e**; 5 W/m^2 in **b**, **d** and 3 W/m^2 in **f**. In the right column magenta contours indicate the 95% significance level. In **e** arrows are shown only where either zonal or meridional wind differences are statistically significant at the 95% level. The significance level is calculated using a two-sample *t* test. The MJO composites are statistically significant in most of the region (95%, one-sample *t* test), except where values are close to zero

For the purpose of this study, a background field is defined as a 15-day average centered 2 weeks before $day_{westerly}$, thus minimizing the potential influence of WWBs on the computation of background winds. Of all 23 wMJO events in the extended winter season, only 2 had WWBs occurring 2 weeks before $day_{westerly}$. Our computations reveal a pronounced warm background SST anomaly (0.5–1 K) in the western-central equatorial Pacific for the wMJO relative to the nwMJO (Fig. 4a), which is not unlike the SST pattern associated with wind bursts observed by Vecchi and Harrison (2000). In our analysis this pattern arises up to a month before the first WWB of the sequence but can also be amplified by subsequent WWBs as the warm pool eastern edge shifts eastward (Lengaigne et al. 2003; Fedorov et al. 2015; Hu et al. 2014; Hu and Fedorov 2017). A patch of anomalous westerly winds (~4 m/s) is observed to the west of the SST anomaly (Fig. 4b).

Computing the composite background SST relative to the daily climatology during the wMJO would yield similar SST patterns but of smaller (roughly by half) amplitudes (Fig. S5a). The composite background surface winds relative to the daily climatology also exhibit westerly wind anomalies (~2 m/s) to the west of the warm SST anomaly, but there are significant easterly wind anomalies off the equator, which are not present in Fig. 4b. This is because the western-central equatorial Pacific experiences the easterly phase of the wMJO, which manifests in Fig. S5b. In contrast, in Fig. 4b easterly wind anomalies associated with the wMJO and nwMJO almost cancel each other when we calculate the difference between the wMJO and nwMJO composites of background zonal surface winds. That is why the approach used in Fig. 4 and later in Fig. 10, i.e., subtracting the wMJO and nwMJO composites, is preferable to subtracting the climatology from the wMJO composites. We estimate the background westerly wind anomalies during the wMJO is about 2 m/s, which is below the WWB threshold. Moreover, later we show that the majority of WWBs are associated with the MJO or tropical cyclones, which indicates that the effect of SST on WWBs has to be indirect.

The causes of these background SST and the corresponding zonal wind anomalies remain under study. They may be related to the North Pacific meridional mode (Chang et al. 2007) or could be of stochastic origin. Regardless of their causes, this warm SST anomaly over the central equatorial Pacific with westerly wind anomalies to its west could enhance convection in this region and modify the MJO structure during the onset stage of El Niño in a way that facilitates the generation of WWBs. This is further confirmed by a

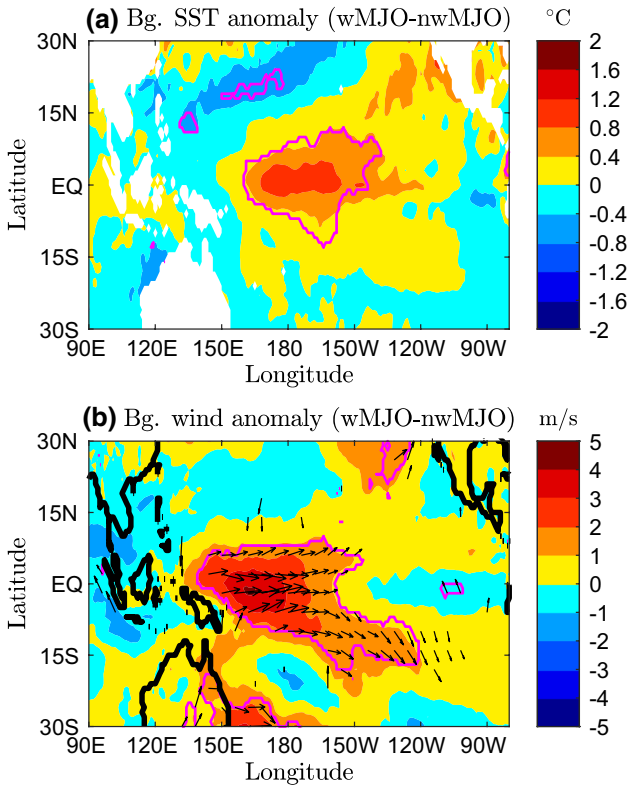

Fig. 4 Extended winter season (DJFMA) composite differences of background **a** SST and **b** surface zonal wind fields between the wMJO and nwMJO events in color shading. These composites are based on the same MJO events as used in Fig. 3. Background fields are defined using a 15-day mean centered 14 days before $day_{westerly}$. Magenta contours indicate the 95% significance level and arrows in **b** are shown only where zonal or meridional wind differences are statistically significant at the 95% level. The plot indicates that during this season, prior to wMJO events, there typically develops a background SST anomaly in the central-western Pacific relative to nwMJO events (with the corresponding background westerly winds). Similar but by about half weaker background anomalies can be seen with respect to the daily climatology (Fig. S5)

complementary modeling study by Liang et al. (2020) which superimposed this SST anomaly in an atmospheric model producing a realistic MJO.

Seiki and Takayabu (2007b) analyzed atmospheric energetics to show that the observed background westerly wind anomalies could draw synoptic-scale disturbances closer to the equator during the westerly phase of the MJO, which is essential for WWB generation. Here, we go further and compare tropical cyclone tracks during the westerly phases of the wMJO and nwMJO. Figure 5 shows TC tracks during the selected 16 wMJO events and 18 nwMJO events—the tracks observed during the interval that starts five days before and ends five days after $day_{westerly}$ are plotted. As we consider the extended winter season (DJFMA), TCs in Fig. 5a, b develop mostly in the southern hemisphere with only a few in the western North Pacific. Calculating the mean longitudinal and latitudinal locations of tropical cyclones in the South Pacific, we find that during the westerly phase of the wMJO, tropical cyclones in the western-central South Pacific become significantly closer to the equator and displaced eastward (at a 95% significance level) compared to the nwMJO with average 1.2° equatorward and 7° eastward shifts (Fig. 5c). In the northern hemisphere, even though tropical cyclogenesis is less frequent, we see an eastward shift of TCs during the westerly phase of the wMJO. As the climatological wind is easterly in the central-eastern equatorial Pacific compared to westerly in the western equatorial Pacific (Fig. S4b, d), the eastward displacement of TCs facilitates WWB generation there. Those TCs in the relative vicinity of the equator, together with westerly wind anomalies of the wMJO can then generate strong WWBs. The eastward displacement of TCs also suggests that the MJO during the onset stage of El Niño may shift eastward as well.

Note that the enhanced tropical cyclone activity near the equator in Fig. 5c is consistent with the enhanced MJO convection in the same region (Fig. 3e, f), suggesting the role of the MJO in modulating TC activity (e.g., Camargo et al. 2009). Furthermore, we find that on average one more TC is generated during each selected wMJO event compared to the nwMJO event, which may be related to larger amplitudes of the selected wMJO. It is also possible that the warm SST and background westerly wind anomalies in the central equatorial Pacific could directly enhance the cyclogenesis, even though previous studies found correlation only between the cyclogenesis location and the Southern Oscillation index (e.g., Revel and Goulter 1986; Hastings 1990), rather than the number of generated TCs.

We can also compare the potential contribution to WWBs from the background westerly wind anomalies and that from the MJO and TCs. These background wind anomalies on the equator reach about 2 m/s; adding them to wMJO westerly wind anomalies of about 2 m/s (Fig. 3a) gives 4 m/s, which is below the threshold in the WWB definition. As maximum zonal wind anomalies of the WWB can sometimes reach 10 m/s or even more (Fig. 2a), the contribution from TCs can be as large as 6 m/s.

Next, we show two examples of MJO events with embedded TCs—one that generated westerly wind bursts and the other one that did not (Fig. 6). On February 23rd of 2014, in the absence of tropical cyclones, a wMJO has already initiated a WWB (Fig. 6a). A few days later, on February 27th, a pronounced tropical cyclone was observed near 10°N, and another one emerged near 10°S on March 3rd. The westerly wind anomalies of the wMJO and two embedded TCs caused a strong and persistent WWB. In contrast, during the nwMJO event in March 2013 (Fig. 6d–f), which was even stronger than the wMJO in February, the filtered OLR anomalies were elongated northwest-southeast, so that westerly

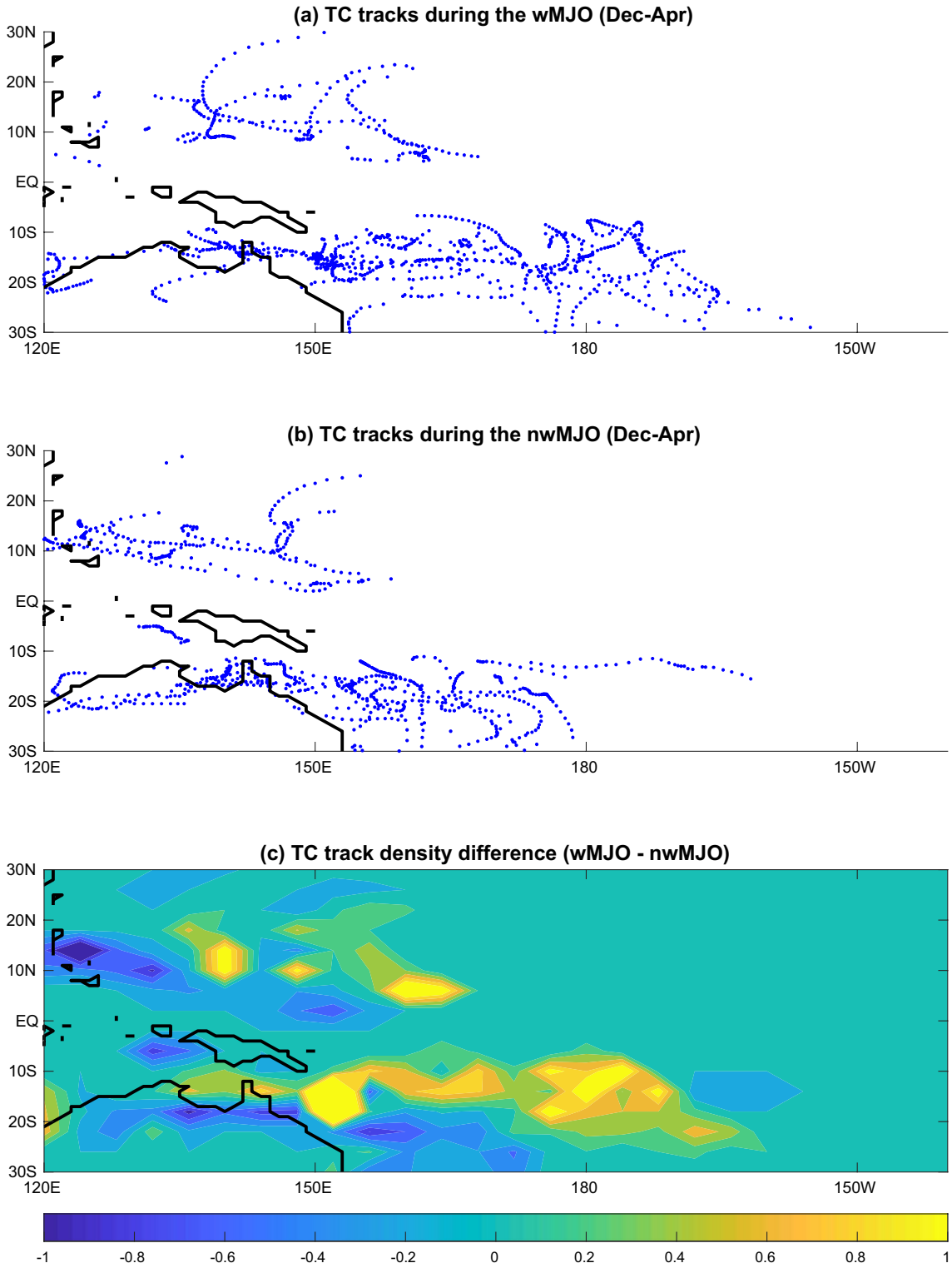

Fig. 5 Tropical cyclone (TC) tracks during the westerly phase of **a** 16 wMJO events and **b** 18 nwMJO events in the extended winter season (DJFMA). The composites are based on the same MJO events as used in Fig. 3. Blue dots indicate TC locations during the interval between 5 days before and 5 days after $day_{westerly}$. **c** Difference in the TC track density between **a** and **b**. The number of TCs are averaged within 4° by 4° boxes and among selected MJO events. The contour interval is 0.2 TC per gird box per MJO event. Note the intensification, and the equator-ward and eastward shift of southern hemisphere TCs during the wMJO events, which favor WWBs

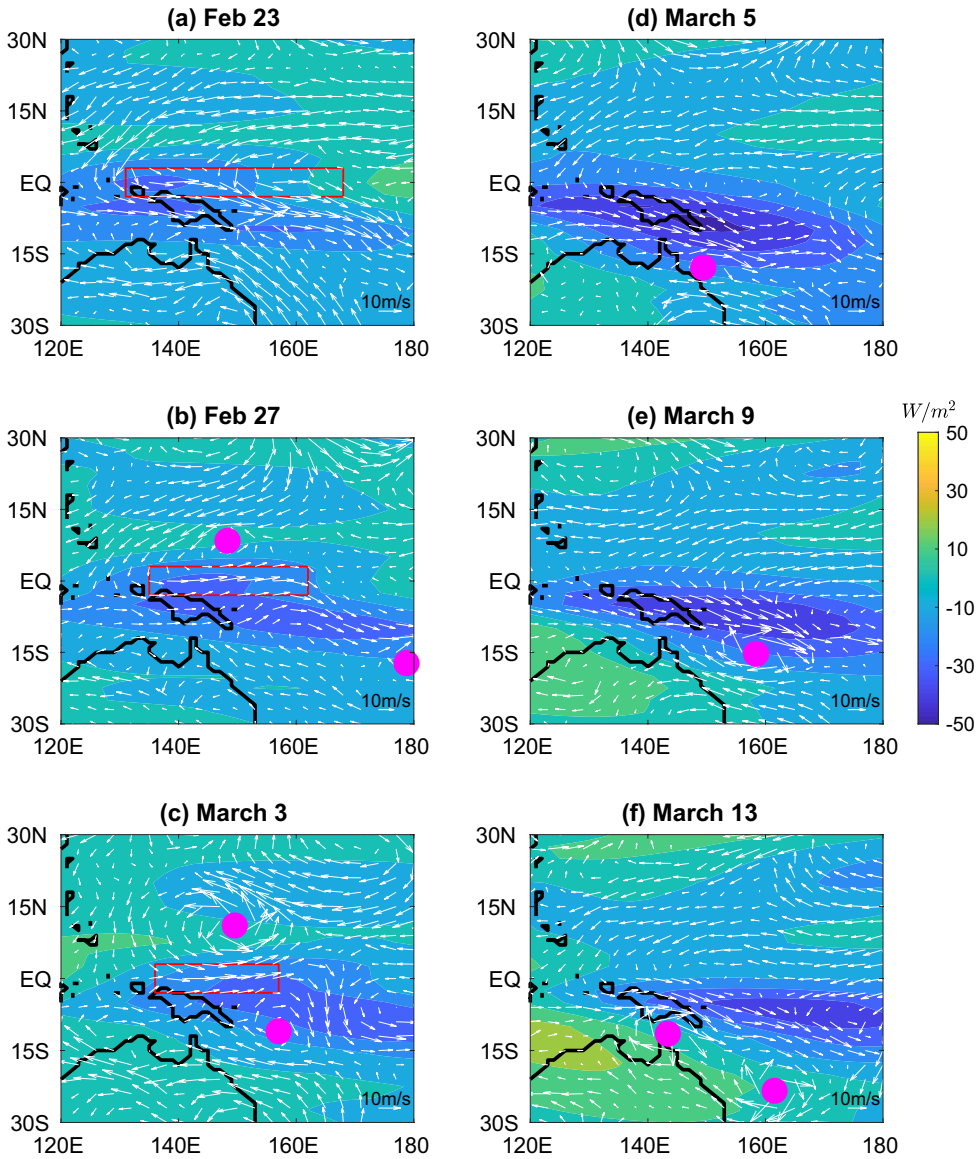

Fig. 6 Snapshots of the filtered OLR field and tropical cyclones embedded in the westerly phase of **a**–**c** one wMJO event in the spring of 2014 compared to **d**–**f** another nwMJO event in the spring of 2013. Color shading indicates band-pass space–time filtered OLR anomalies (zonal wavenumbers 1–5, periods between 30–95 days) with the color shading interval of 10 W/m^2. White arrows indicate raw wind vectors at 1000 hPa, and solid magenta dots mark the centers of tropical cyclones. The white arrow in the bottom right corner of each panel gives a 10 m/s scale. Red boxes in the left panels indicate the region where the WWB was identified. Note that to generate WWBs a TC should pass sufficiently close to the equator

wind anomalies in the equatorial band were much weaker. One TC was generated within the negative OLR anomalies near 15°S on March 5th, and another one was observed on March 13th. However, as TCs developed sufficiently far away from the equator, no WWBs were generated. This suggests that only under favorable environmental conditions (e.g., background warm SST and westerly anomalies), can strong MJO events with embedded TCs generate WWBs, which is consistent with the findings of Seiki and Takayabu (2007b) and is further validated by numerical experiments of Liang et al. (2020).

The temporal evolution of the WWB intensity (ano_{day}) and the maximum U1000hPa anomaly averaged between 3°N–3°S for the wMJO in Fig. 6 is shown in Fig. 7. The WWB started on February 16th due to westerly wind anomalies of the wMJO (WWB criteria 1 and 2 were met) and then maintained a relatively strong magnitude for a week or so. Then two cyclonic disturbances emerged near the equator on February 24th (these disturbances were recorded in the best track dataset on February 27th). These TCs gradually intensified and the WWB reached the maximum U1000hPa anomaly on March 3rd. Later on, with the decay of the MJO and southward drift of TCs, the WWB gradually weakened and ended on March 6th. We estimate the correlation coefficient r = 0.63 between the WWB intensity and the maximum U1000hPa anomaly, indicating the WWB amplitude largely depends on the strength of U1000hPa anomalies on the equator.

The analysis in Figs. 6 and 7 demonstrate how the MJO with embedded TCs generates westerly wind bursts. Note

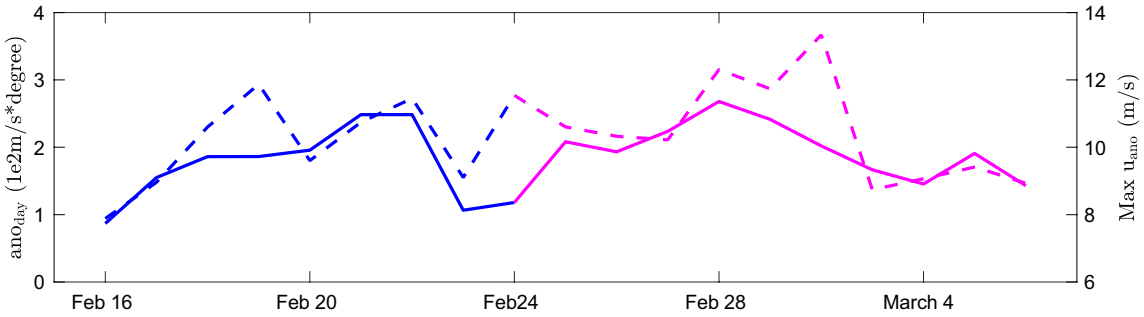

Fig. 7 Temporal evolutions of the spatially-integrated U1000hPa anomalies (solid line, computed from Eq. 1) and the maximum U1000hPa anomaly averaged between 3°N–3°S (dashed line) for the wind burst generated by the wMJO event shown in Fig. 6a–c. Blue indicates the period when the WWB was generated solely by the MJO and magenta indicates the period when the WWB was generated by the MJO but with a strong contribution from embedded TCs. This WWB was initiated by the MJO around Feb 16th. TCs were generated in the vicinity of the equator on Feb 24th but not recorded in IBTrACS until 27th. The TCs' contribution to the WWB continued until the burst termination on March 6th

that during WWBs, TCs may be present and remain sufficiently close to the equator only for a limited time, which is the case during the initial period of the burst discussed above. We also point out that while we focus on how the MJO with embedded TCs generates WWBs, other weather systems can also be involved in this process. For example, Puy et al. (2016) finds that 41% of WWBs are associated with the co-occurrence of the MJO and convectively coupled Rossby waves (CRWs). In this study, the weather systems like CRWs are not investigated but their role in generating WWBs is not excluded.

In total, 34 WWBs are identified from December to April (El Niño decay periods are excluded) during the studied period (1979–2016). Most of these bursts are generated by MJO events with embedded TCs, while a few are generated solely by the MJO or TCs and the rest are not associated with either of them, as summarized in Fig. 8 and Table 1. Here, we consider that a tropical cyclone generates a WWB if the TC is involved in the generation for more than 3 days. Among the 34 WWB events, 25 (74%) are caused by the combined effect of the MJO and TCs, and 2 are generated by the MJO only. Moreover, we find that WWBs caused by the MJO with embedded TCs are typically much stronger than wind bursts caused by other mechanisms (Fig. 8). This suggests that the MJO with embedded TCs is the most important mechanism for generating WWBs during the onset stage of El Niño.

3.2 WWBs in the extended summer season

WWBs also occur over the western and central equatorial Pacific during the extended summer season (MJJASON) when El Niño develops rapidly and its growth depends on the Bjerknes feedback (Bjerknes 1969; Zebiak and Cane 1987; Seiki and Takayabu 2007a; Jin et al. 2006; Hu and Fedorov 2017). Warm equatorial SST anomalies during this time are strengthened by the thermocline and zonal advection feedbacks (Vecchi and Harrison 2000; Fedorov et al. 2015) and WWBs can be critical for maintaining the growth of anomalies. In 2014, the lack of WWBs and the generation of easterly wind bursts interrupted El Niño development, which resulted in a very weak warm event of 2014, barely over the El Niño threshold (Hu and Fedorov 2016; Puy et al. 2017; Seiki et al. 2018). In this section, we will again use a composite analysis to investigate how the MJO with embedded TCs can generate WWBs but now during the extended summer season (El Niño decay periods are excluded), when we identify 26 wMJO and 32 nwMJO events in total. Top 34 MJO events are selected during this period, depending on Amp_{MJO}, among which 13 are wMJO events and 21 are nwMJO events. If all MJO events during this period were considered, the results would be similar except that the significance level of the difference between the wMJO and nwMJO would be slightly reduced.

The composite space–time filtered wind speed anomalies at 1000 hPa and OLR anomalies on $day_{westerly}$ for these wMJO and nwMJO events are compared in Fig. 9 (first and second columns, respectively). The MJO during this period is weaker than during boreal winter and spring, with a limited influence on the equatorial band near the dateline (c.f., Fig. 3). Nevertheless, significantly stronger westerly wind and negative OLR anomalies are observed over the central equatorial Pacific for the wMJO, as compared to the nwMJO. Furthermore, a reduction of convective activity, even though not as significant, is also observed over the western North Pacific for the wMJO (Fig. 9f). This indicates the southeastward shift of convective activity within the wMJO and an enhancement of convective activity over the central equatorial Pacific, which facilitates the generation of WWBs. Note the significance level of the difference between the wMJO and nwMJO is lower than that for the winter-spring season, implying that the MJO plays a somewhat less

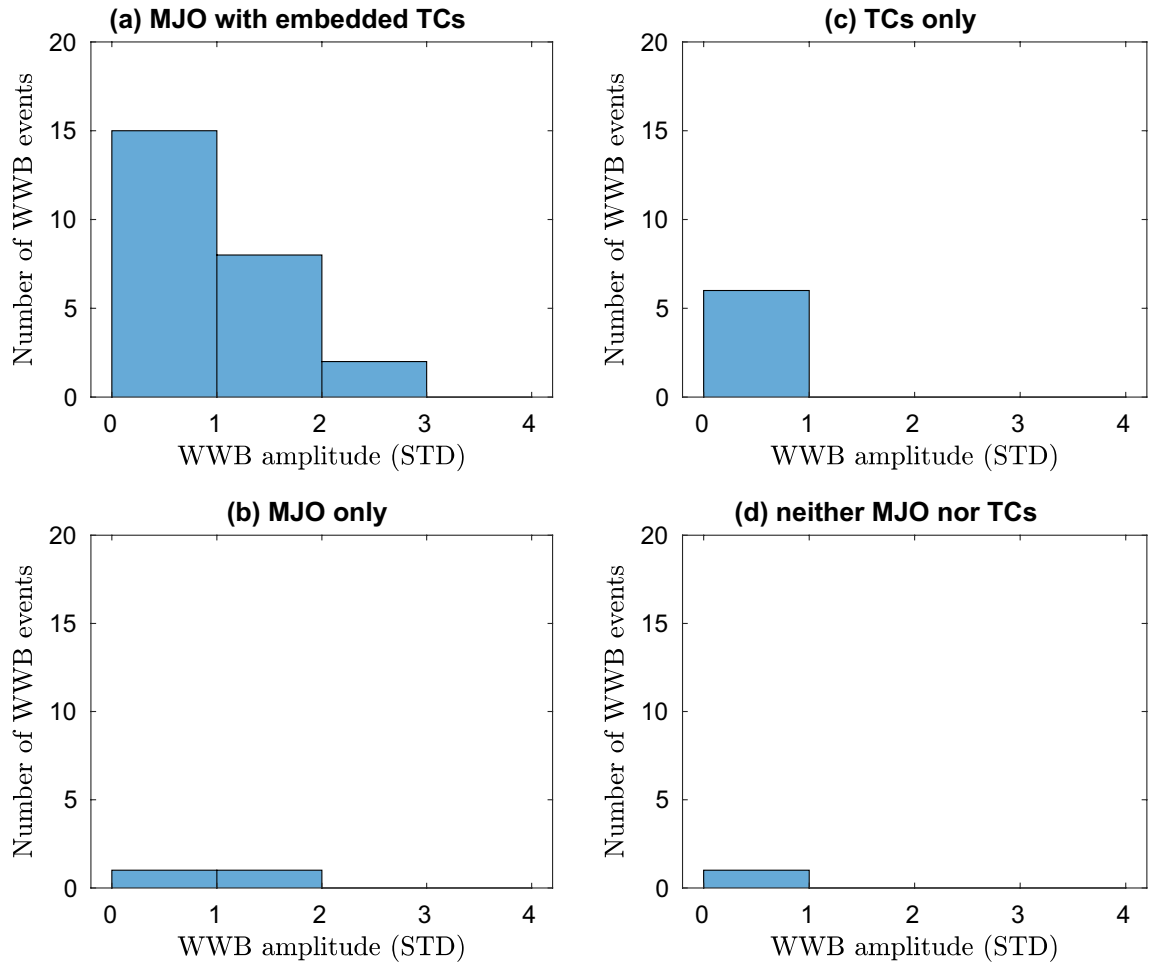

Fig. 8 Histograms showing the distribution of WWB amplitude for bursts generated by **a** MJO events with embedded TCs, **b** MJO only, **c** TCs only, and **d** neither MJO nor TCs, all for the extended winter season (December through April; estimated for years 1979–2016 with El Niño decay periods excluded). In total, 34 WWBs are identified during this period. 1STD = 2430 m/s*degree*day, which is the standard deviation of Amp_{wwb} for all WWBs summarized in Tables 1 and 2. This unit gives a measure of WWB amplitude after integrating U1000hPa anomalies over longitude and time

Table1 The total numbers of westerly wind bursts generated by MJO events with embedded TCs, by MJO or TCs only, and by neither MJO nor TCs in the extended winter season (December to April, for years 1979–2016 with El Niño decay periods excluded)

MJO with embedded TCs	MJO only	TCs only	neither MJO nor TCs
25	2	6	1

Note that even when the MJO or TCs are the primary causes of WWBs, other processes may have also contributed to the generation of these WWBs

important role in WWB generation during the development stage of El Niño as compared to El Niño onset. This is further confirmed by the analysis to follow. In addition, since MJO events in October and November has features of both the wintertime and summertime MJO, the inclusion of these MJO events in the MJJASON composites can also reduce the significance level. In Fig. S6, which shows the MJJAS composites of the wMJO and wMJO, the difference between the two composites is slightly more significant.

Computing the difference between the wMJO and nwMJO composites of background SST and wind fields (Fig. 10) reveals a warm SST anomaly (up to 2 K) extending into the eastern equatorial Pacific that precedes WWBs by several weeks. The composite background SST and zonal surface winds during the wMJO and nwMJO are also shown in Fig. S7 for reference. This warm SST anomaly can be caused by the prior WWBs of the early season and is amplified by the Bjerknes feedback (McPhaden 1999; Vecchi and Harrison 2000; Fedorov 2002). A persistent patch of anomalous westerly winds (up to 3 m/s) is also observed to the west of this SST pattern. These SST and wind anomalies signify the development of El Niño conditions. Of all 26 wMJO

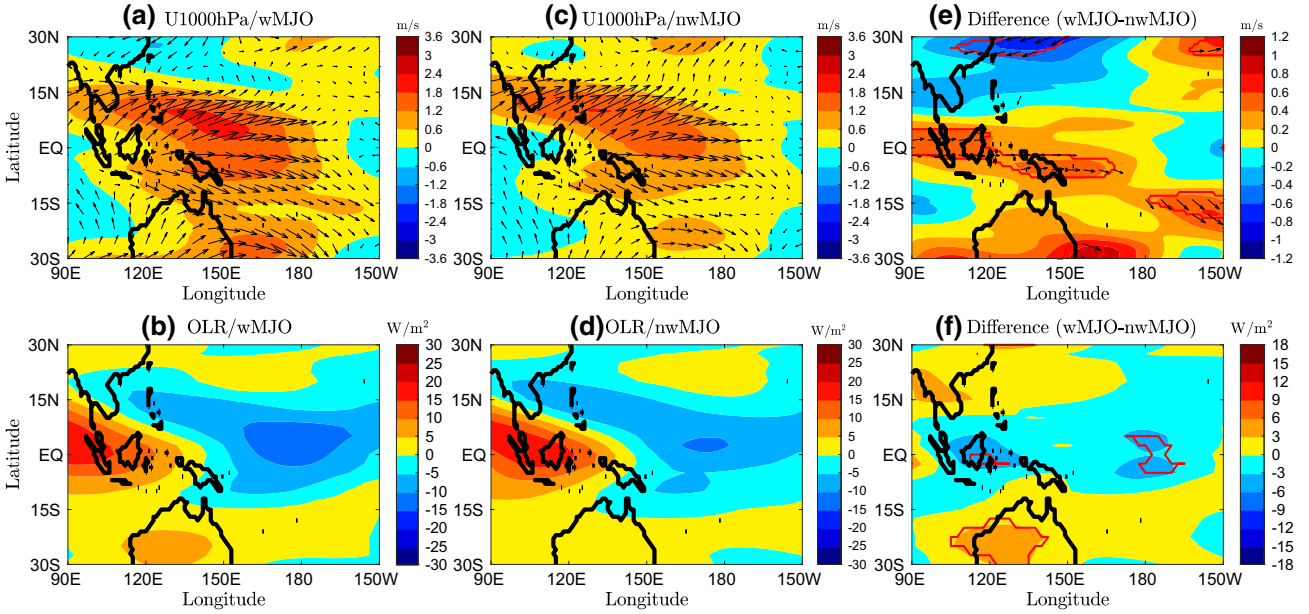

Fig. 9 As in Fig. 3 but for 13 wMJO and 21 nwMJO events during the extended summer season (May to November). Red contours in panels (**e**) and (**f**) indicate the 90% significance level

events in the extended summer season, only 2 had WWBs occurring already 14 days before $day_{westerly}$, suggesting that WWBs have a minimal influence on our computation of background wind fields.

Additional calculation of the composite background SST and zonal wind anomalies but relative to the daily climatology during the wMJO yields anomalous SST and westerly winds of around 1 K and 1.5 m/s, respectively (Fig. S8). This patch of westerly wind anomalies is much weaker than the WWB threshold, and by itself cannot generate WWBs. We hypothesize that these background warm SST and westerly wind anomalies cause the enhancement of the MJO over the central equatorial Pacific, which contributes to the generation of WWBs. This role of background SST and westerly wind anomalies is further confirmed by a complementary study that utilizes an atmospheric GCM with a realistic MJO (Liang et al. 2020).

TC tracks during the westerly phase of the wMJO and nwMJO events are displayed in Fig. 11a, b, which show tropical cyclone tracks within the interval 5 days before and 5 days after $day_{westerly}$. During the westerly phase of the nwMJO, most of TCs generated in the western North Pacific are to the west of 150°E. Those TCs are generated in a region where seasonal mean zonal winds are westerly (c.f., Fig. S7d) and their locations are sufficiently far away from the equator, so WWBs rarely happen. In contrast, during the westerly phase of the wMJO, TCs embedded in the MJO are found farther east where seasonal mean winds are easterly (c.f., Fig. S7b), and closer to the equator due to the enhancement of the wMJO over the central equatorial Pacific. Calculating the mean longitude and latitude of tropical cyclones in the North Pacific in Fig. 11a, b, we find that the mean location of tropical cyclones during the westerly phase of the wMJO shifts about 4.5° equatorward and 9.9° eastward (at a 95% significance level) as compared to the nwMJO. Consequently, more TCs are observed between 150°E and 180°, where WWBs usually happen. The southeastward shift of TC tracks in the northern Pacific is evident in Fig. 11c. These tropical cyclones sufficiently close to the equator together with westerly wind anomalies of the MJO induce strong WWBs during the development stage of El Niño.

Examples of wMJO and nwMJO events that occurred in summer are shown in Fig. 12 (for the years 2015 and 2016). In the early summer of 2015, with the development of El Niño, warm SST anomalies of about 2 °C extended from the central to the eastern equatorial Pacific (Hu and Fedorov 2017), allowing an wMJO event to develop with a strong convective signal along the equator (Fig. 12a–c). On June 27th, westerly wind anomalies of the wMJO initiated the WWB in the absence of TCs. On July 1st, two clearly defined TCs emerged not too far from the equator, with centers at around 10°N and 10°S. These twin cyclones, nearly symmetric with respect to the equator, intensified the westerly wind burst in the equatorial band. The WWB then gradually weakened with now three TCs north of the equator drifting poleward. These TCs in the vicinity of the equator and westerly wind anomalies of the wMJO induced a strong and prolonged WWB. In contrast, during

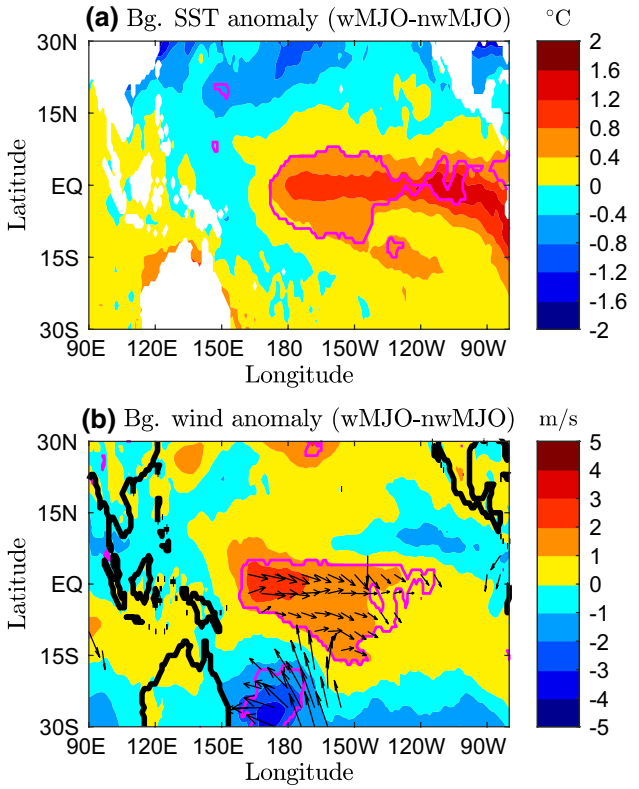

Fig. 10 As in Fig. 4 but for the extended summer season (May through November). These composites are based on the same MJO events as used in Fig. 9. The plot indicates that during this season, prior to wMJO events, there typically develops a background equatorial SST anomaly in the central-eastern Pacific relative to nwMJO events (with the corresponding background westerly winds). Similar but a slightly weaker background anomalies can be seen with respect to the daily climatology (Fig. S8). While the largest background SST difference is seen in the eastern equatorial Pacific and is associated with the developing El Niño, it is the central Pacific anomaly that is critical for WWB generation

the nwMJO event in 2016 (Fig. 12d–f), negative OLR and westerly wind anomalies of the MJO were centered around 15°N with a weak signal over the central equatorial Pacific. Two TCs embedded in this nwMJO event were generated around 15°N. As TCs were farther away from the equator, no WWBs occurred.

Figure 13 shows the temporal evolution of the WWB intensity and the maximum U1000hPa anomaly for the burst shown in Fig. 12a–c. This WWB started on June 26th and its intensity remained relatively low for a few days. Staring on June 29th, several TCs emerged near the equator including the twin TCs (Fig. 12b), which at first strengthened the WWB. However, with the northward drift of the northern TCs, the WWB gradually weakened. On July 7th, when the first TCs drifted away from the equator, the WWB intensity reached its minimum. In the meantime, a new TC emerged east of the dateline and close enough to the equator. As the seasonal mean winds in this region are easterly, this TC greatly enhanced the WWB intensity until the decay of the MJO and northward drift of the TC. We again find that the WWB intensity is highly correlated with the maximum U1000hPa anomalies on the equator (r = 0.81).

In total, 63 WWB events are identified during the extended summer season in 1979–2016 (May to November, El Niño decay periods excluded). 24 WWBs (38%) are generated by the MJO and embedded TCs (Table 2 and Fig. 14), which is significant but smaller than the number during the onset stage of El Niño (74%). WWBs not associated with the MJO account for 54%, indicating that the MJO is less important in generating WWBs during the development stage of El Niño compared to the earlier onset. In addition, during the development stage, WWBs generated by TCs alone are of similar strength to those generated by the MJO with embedded TCs, suggesting other mechanisms may be of equal importance for WWB generation. This finding is related to a weaker MJO activity during boreal summer and fall than in winter and spring, while other convectively coupled disturbances like convectively coupled Rossby waves may become more active (Wheeler and Kiladis 1999). Finally, the MJO during this time has a generally weaker signal over the central equatorial Pacific, especially between May and September when the MJO convective activity is shifted away from the equator, which does not favor WWB generation (c.f. Fig. 9).

3.3 The dependence of WWB amplitude on background SST and westerly wind anomalies

As shown by the above analyses, the background warm SST and westerly wind anomalies appear to be vital for wind burst generation. The SST-dependency of WWBs has been examined in a number of studies (e.g., Kessler 2001; Tziperman and Yu 2007; Kug et al. 2008; Levine and Jin 2017). However, most of these studies have neglected the seasonality of the WWB relationship with background SST/wind anomalies over the entire El Niño cycle. To that end, in this section we aim to quantify the dependence of WWB amplitude (Amp_{wwb}) on background SST and westerly wind anomalies, stratified by different seasons.

To measure the average magnitude of anomalous background SST and westerly winds during the extended winter season, we define Ano_{sst} and Ano_u, as background SST and U1000hPa anomalies relative to the climatology averaged in 150°E–170°W, 6°N–6°S and 130°E–170°, 6°N–6°S, respectively. Similarly, Ano_{sst} and Ano_u during the extended summer season are defined as background SST and U1000hPa anomalies averaged in 170°E–120°W, 6°N–6°S and 130°E–180°, 6°N–6°S, respectively. The averaging regions correspond to where these background warm

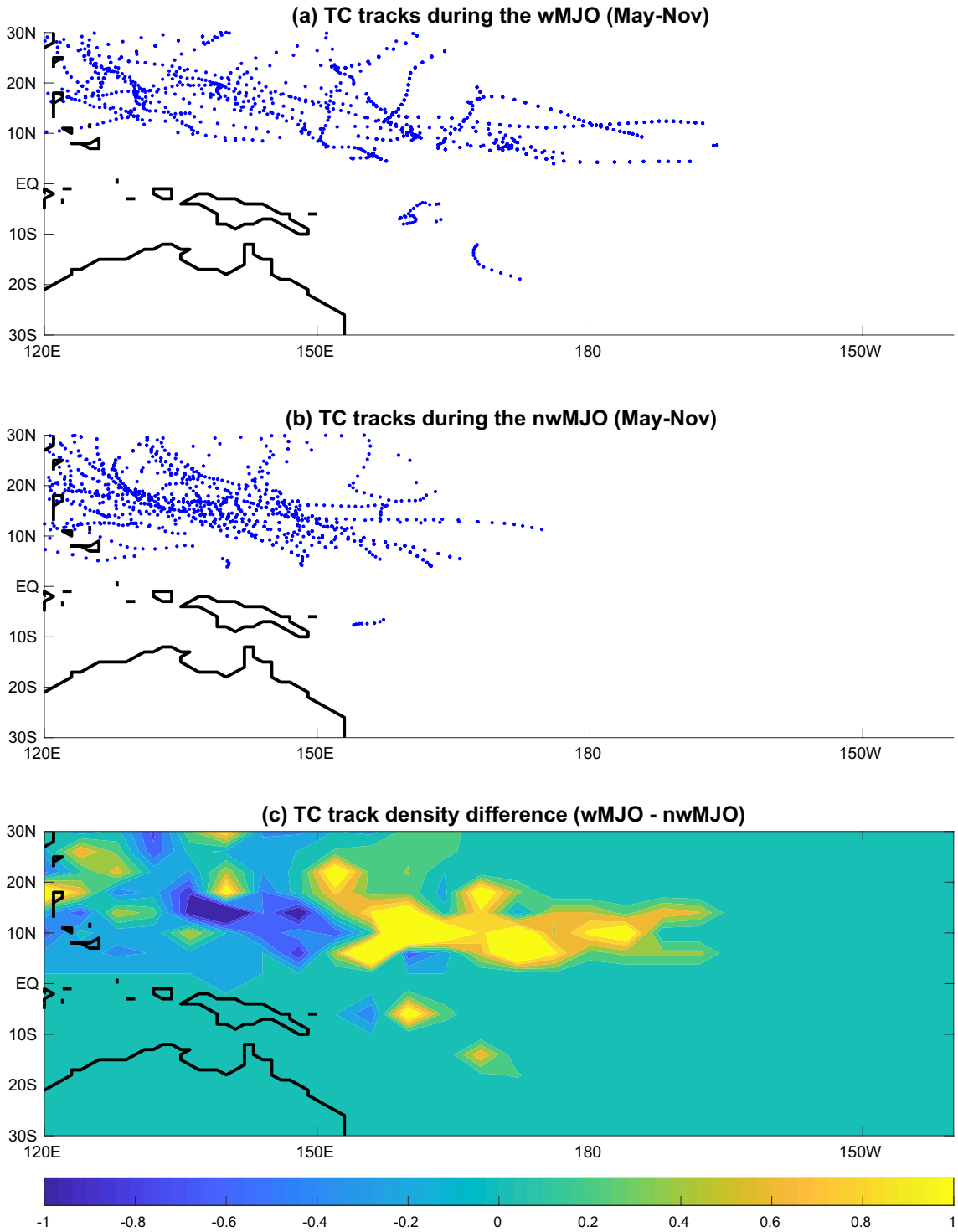

Fig. 11 As in Fig. 5 but in the westerly phase of **a** 13 wMJO events and **b** 21 nwMJO events during the extended summer season (May through November). Note that the intensification, and the equatorward and eastward shift of TC activity in the northern hemisphere during the wMJO events favor WWBs

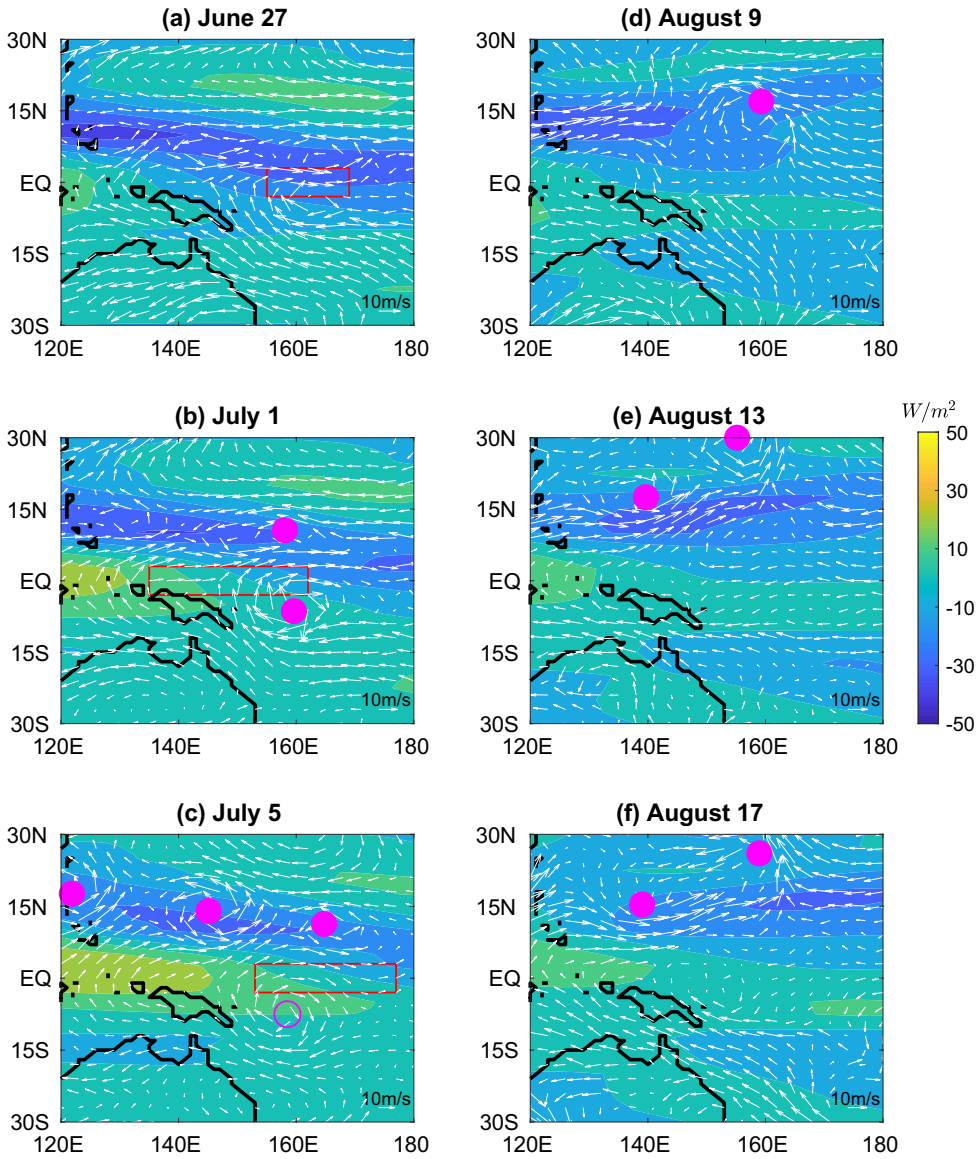

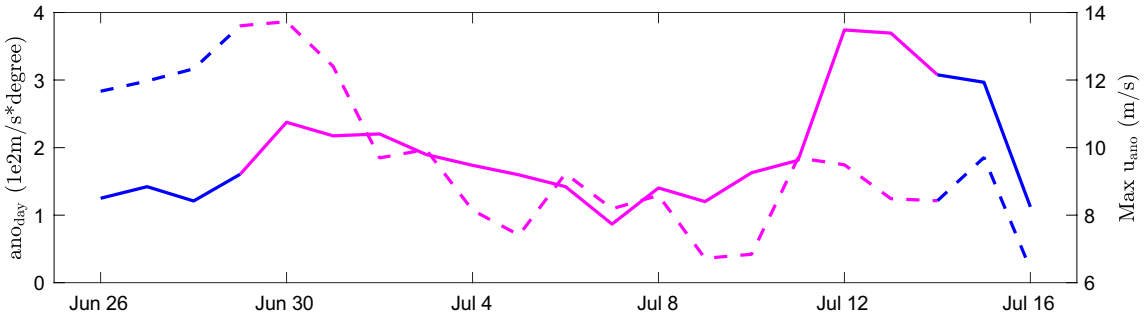

Fig. 12 As in Fig. 6 but for **a**–**c** one wMJO event in the summer of 2015 and **d**–**f** another nwMJO event in the summer of 2016. The TC observed south of the equator in **b** later became a tropical disturbance marked as an open circle in **c**, which was not recorded in the IBTrACS dataset

Fig. 13 Temporal evolutions of the spatially-integrated U1000hPa anomalies (solid line) and the maximum U1000hPa anomaly averaged between 3°N–3°S (dashed line) for the wind burst generated by the wMJO displayed in Fig. 12a–c. Blue indicates the period when the WWB was generated solely by the MJO and magenta indicates the period when the WWB was generated by the MJO but with a strong contribution from embedded TCs. The WWB was initiated by westerly wind anomalies of the MJO on June 26th. TCs emerged in the vicinity of the equator on Jun 29th and enhanced the burst. The WWB intensity then gradually weakened until Jul 7th when a new TC was generated near the equator. Between July 14th and 16th, no clear-defined TCs were involved in the maintenance of this wind burst

Table 2 The numbers of westerly wind bursts generated by MJO events with embedded TCs, by MJO or TCs only, and by neither MJO nor TCs in the extended summer season (May to November; years 1979–2016 with El Niño decay periods excluded)

MJO with embedded TCs	MJO only	TCs only	neither MJO nor TCs
24	5	25	9

Note that even when the MJO or TCs are the primary causes of WWBs, other processes may have also contributed to the generation of these WWBs

SST and westerly wind anomalies are centered (Figs. S5 and S8). As we have tested, expanding or contracting the averaging regions by about 10° of longitude would not affect the analysis to come. However, as discussed before, we need to keep in mind that Ano_u includes some MJO easterly wind signals, which may affect a little the analysis of the relationship between Amp_{wwb} and Ano_u.

We note that in several cases more than one WWB occurred during the westerly phase of a wMJO, and in such cases the amplitudes Amp_{wwb} of these WWBs are summed together to give the net WWB amplitude corresponding to a single wMJO event. As mentioned before, in total 23 and 26 wMJO events are identified from December to April, and from May to November in 1979–2016, respectively, with El Niño decay periods excluded.

Figure 15 shows the scatterplots of Amp_{wwb} versus Ano_{sst} and Ano_u for the wMJO events during the extended winter and summer seasons. During the extended winter season, corresponding to the onset stage of El Niño, even though the WWB amplitude does not correlate with background SST anomalies, the large majority of WWBs occur for positive background SST anomalies ranging between 0.1 and 0.6 K. At the same time, the WWB amplitude is positively correlated with background wind anomalies (r = 0.37 at the 90% confidence level). In part, this positive correlation is due to the contribution of background wind anomalies to WWBs (see previous discussion). These

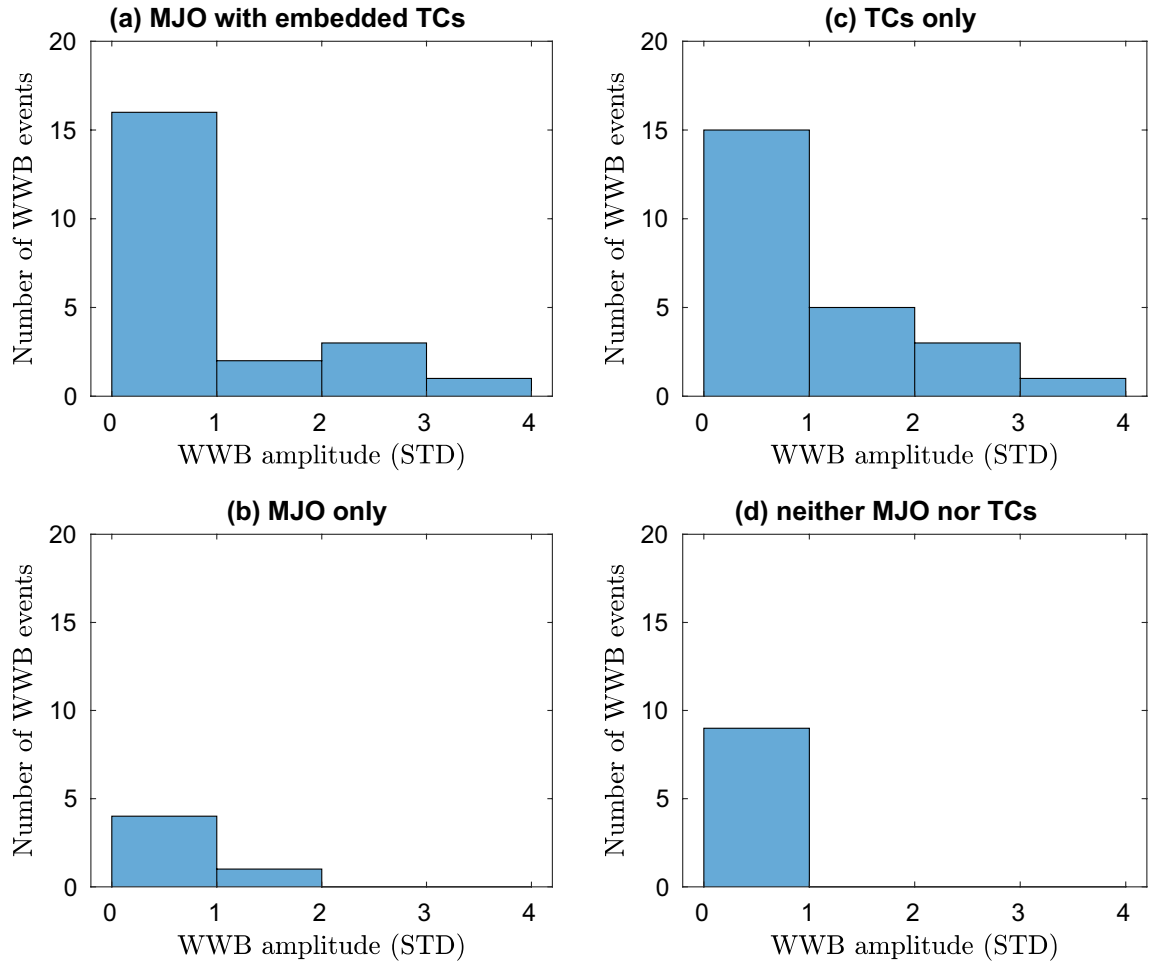

Fig. 14 As in Fig. 8 but for the extended summer season (May through November, estimated for years 1979–2016 with El Niño decay periods excluded). In total, 63 WWB events have been identified for this period

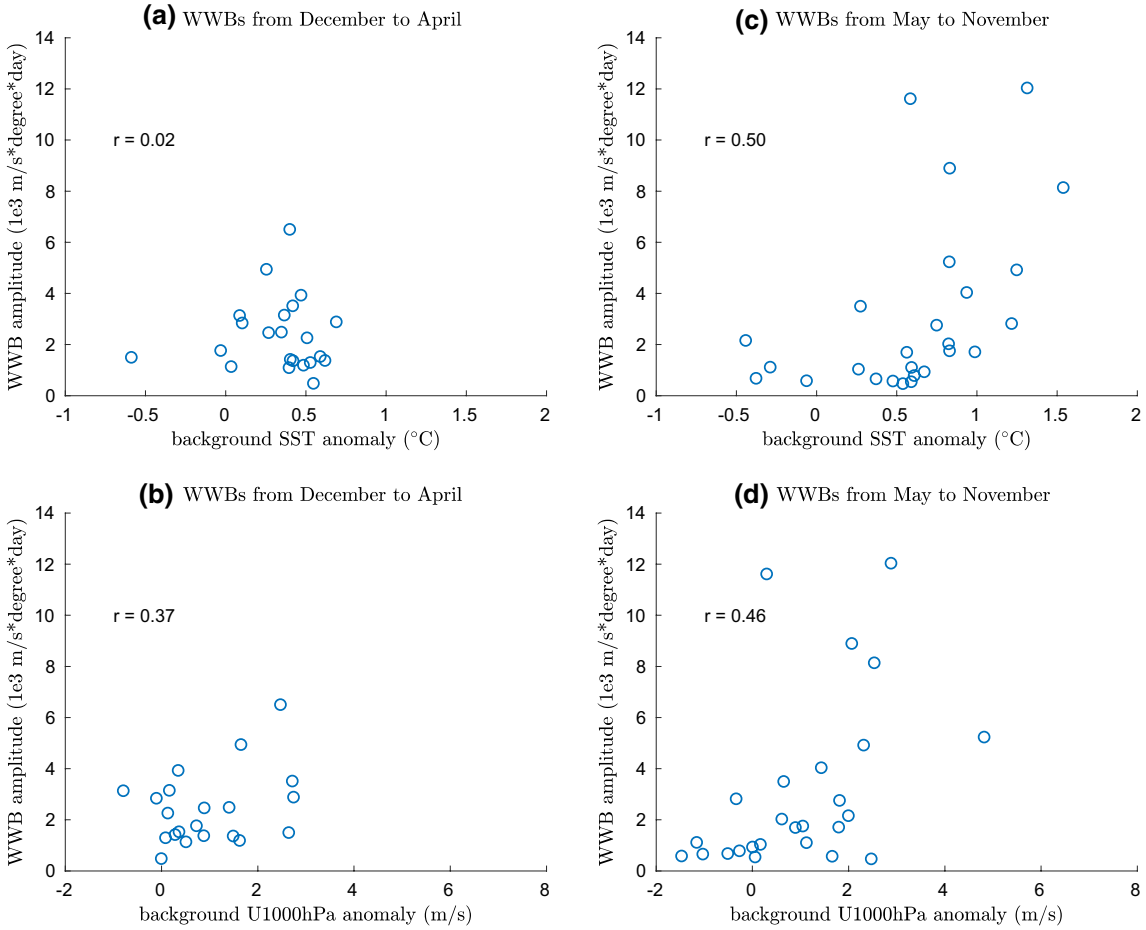

Fig. 15 Scatterplots of westerly wind burst amplitude (Amp_{wwb}) versus (**a**, **c**) background SST and (**b**, **d**) background U1000hPa anomalies for WWBs generated by the wMJO. Left column: December through April; right column: May through November, for years 1979–2016 with El Niño decay periods excluded. Correlation coefficients are also shown. Background fields are defined using a 15-day mean centered 14 days before $day_{westerly}$. Note that in **a**, **b** we excluded one WWB generated by the wMJO whose $day_{westerly}$ is Jan 12th, 1979. The correlation coefficients in **c** and **d** are both significant at the 95% confidence level. The correlation coefficient in **b** is significant at the 90% confidence level. While there is no correlation in **a**, the vast majority of WWBs occurred when background SST anomalies were between 0.1 and 0.6 °C. The dependence of WWB amplitude on the background SST/wind anomalies becomes nonlinear for large anomalies

results suggest that WWBs during the El Niño onset are more stochastic, but their occurrence still depends on background SST and westerly winds. In contrast, during the extended summer season, corresponding to the development stage of El Niño, the WWB amplitude is positively correlated with both background SST and westerly wind anomalies (r = 0.50 and 0.46, respectively at the 95% confidence level), indicating a stronger state-dependency of WWBs during the development stage of El Niño after May. This is also consistent with the higher predictability of El Niño after the spring predictability barrier has passed (Torrence and Webster 1998; McPhaden 2003).

4 Summary and discussion

Using a composite analysis, we investigate how the MJO with embedded tropical cyclones, modulated by background SST anomalies and corresponding westerly wind anomalies, generates westerly wind bursts (WWBs) in the equatorial Pacific during two seasons – the extended winter (December–April) and extended summer (May–November). These two seasons correspond to the onset and development stages of El Niño respectively, with El Niño decay periods excluded. While WWBs have been linked to the MJO before (e.g., McPhaden et al. 2006b; Hendon et al. 2007; Seiki and Takayabu 2007a, b; Choidi et al. 2014; Puy et al. 2016), the role of variations in the MJO horizontal structure, shown to be crucial for WWB generation in the current study, has been overlooked in those studies. Likewise, most of the

previous studies has not considered the seasonal dependence of the MJO-WWB relationship.

By separating MJO events into two categories—wMJO (generating WWBs) and nwMJO (not generating WWBs)—we are able to highlight significant differences in the horizontal structure between the wMJO and nwMJO events. Additionally, we find that during the extended winter season the MJO is much more important in generating WWBs than during the extended summer season. In fact, about 80% of WWBs generated during the winter season are associated with the MJO versus only 46% during the summer season.

That tropical cyclones or, more generally, cyclonic disturbances can indeed generate WWBs has been observed in a number of previous studies (e.g., Hartten 1996; Harrison and Vecchi 1997; Seiki and Takayabu 2007b; Lian et al. 2018). In particular, during El Niño events there occurs an eastward shift of tropical cyclones in the northwestern Pacific and an equatorward shift in the south Pacific (e.g., Lander 1994; Sobel and Maloney 2000; Revell and Goulter 1986; Hastings 1990; Vincent et al. 2011), and Seiki and Takayabu (2007b) and Lian et al. (2018) suggested that such an equatorward shift of tropical cyclones should be important for WWB generation. In the current study, we confirm their results and find that the eastward shift of tropical cyclones is important as well (e.g., the sharp increase of burst intensity in Fig. 13). Moreover, we estimate that about 70% of WWBs in the extended winter season and 40% of WWBs in the extended summer season are generated by the joint effect of the MJO and embedded tropical cyclones. That is, the majority of MJO-related WWBs are affected by TCs. The intensity of wind bursts generated this way is also much stronger than, or comparable to WWBs generated solely by tropical cyclones in the extended winter and summer seasons, respectively, which suggests that the MJO with embedded tropical cyclones is the most important mechanism for generating WWBs, especially during the extended winter season.

Next, we isolate two background warm SST patterns in the equatorial Pacific critical for WWB generation. These patterns occur during the extended winter and summer seasons, respectively, and arise as part of El Niño onset and further development. They cause changes to the MJO horizontal structure and propagation characteristics, shifting the tracks of tropical cyclones and creating favorable conditions for generating WWBs. A common feature related to those SST patterns is the corresponding background westerly wind anomalies (~ 2 m/s) centered on the equator. Previously, Seiki and Takayabu (2007b) and Seiki et al. (2011) suggested that such winds increase atmospheric eddy kinetic energy near the equator, which favors WWB generation. The effect of background SST and westerly wind anomalies on the MJO horizontal structure and hence the WWB generation is further validated in our companion paper that uses an atmospheric general circulation model (AGCM) simulating a realistic MJO. Thus, the present and the complementary modeling papers allows us to establish a strong link between background SST anomalies emerging as part of El Niño development, the MJO horizontal structure, and the tracks and strength of tropical cyclones. This link facilitates the generation of WWBs.

Specifically, during the extended winter season when the MJO is active mainly in the southern hemisphere, WWB generation is controlled by a warm SST anomaly of about 0.5 K developing in the western-central equatorial Pacific (150°E–170°W, 6°N–6°S). It is not unlike the SST anomaly pattern observed during the onset of El Niño by Vecchi and Harrison (2000). The SST anomaly is accompanied by a patch of background anomalous westerly winds to its west reaching about 2 m/s—most likely a result of convective response to the warmer SST. While the exact causes of these background SST and westerly wind anomalies are debatable, they act to modify the MJO horizontal structure and make it more zonally oriented. This change enhances the MJO convective activity and associated westerly wind anomalies in the equatorial band in the vicinity of the dateline (this result agrees with the observational study of Hendon et al. 2007). Consequently, TC activity in the westerly phase of the MJO is also enhanced especially near the dateline and closer to the equator, contributing to WWB generation.

We note that in addition, El Niño itself can modulate tropical cyclones (e.g., Sobel and Maloney 2000). Furthermore, Vincent et al. (2011) find that warm SST anomalies in the central equatorial Pacific can shift the South Pacific Convergence zone (SPCZ) several degrees of latitude northward thus moving tropical cyclogenesis in the southern hemisphere closer to the equator. Therefore, the observed equatorward and eastward shifts of tropical cyclones embedded in the MJO may be caused by the combined effect of the SPCZ and the MJO responding to SST anomalies. These observations however do not contradict our conclusion that westerly wind anomalies due to the MJO and the MJO-embedded TCs remain the most important mechanism for generating WWBs during the onset stage of El Niño.

We further show that during the extended summer season when the MJO is active primarily in the northern hemisphere, there develops a warm SST anomaly of about 1 K in the central-eastern equatorial Pacific (170°E–120°W, 6°N–6°S) with corresponding westerly wind anomalies ~ 1.5 m/s to its west, which signifies the development of El Niño. The amplitudes here are given in a composite sense. These favorable environmental conditions enhance MJO activity over the central equatorial Pacific, strengthening the MJO-induced westerly wind anomalies in the equatorial band. TCs during the westerly wind phase of the MJO shift eastward and towards the equator, amplifying the original westerly wind anomalies and thereby inducing strong

WWBs. This mechanism of WWB generation accounts for nearly 40% of all WWB events during this period. Overall, during this time, WWBs caused by separate tropical cyclones appear to be of similar strength as WWBs generated by the MJO with embedded TCs.

Note that while we focus on how the MJO with embedded TCs generates WWBs, other atmospheric intra-seasonal oscillations may also be involved in this process, including convectively coupled Rossby waves (CRWs) (Seiki and Takayabu 2007b; Puy et al. 2016). In fact, the large-scale structure of twin tropical cyclones seen in Fig. 12b resembles that of a quasi-stationary Rossby wave that one would expect from a Gill-type response to an atmospheric heating centered on the equator (Gill 1980; Matsuno 1966). Future studies will be needed to understand the interaction between these processes in more depth.

Finally, the relationship between the amplitude of WWBs and the early year background SST anomalies raises the question of stochastic versus state-dependent behavior of WWBs. That WWBs can act as multiplicative noise during the development of El Niño has been recognized in a number of studies (e.g., Eisenman and Tziperman 2005). Here, we show that even during the early stages, while the amplitude of wind bursts remains largely stochastic, the WWB occurrence still depends on background SST and westerly winds, with the majority of bursts occurring during favorable background conditions. During the subsequent development stages of El Niño, the state dependence of WWB amplitude becomes even more evident.

Supplementary Information The online version contains supplementary material available at https://doi.org/10.1007/s00382-021-05757-1.

Acknowledgements This research was supported by grants to A.V.F. from NSF (AGS-1405272), NASA (NNX17AH21G) and NOAA (NA20OAR4310377).

Data availability The datasets generated during and/or analysed during the current study are available in the ERA-interim dataset, [https://www.ecmwf.int/en/forecasts/datasets/reanalysis-datasets/era-interim]; Oceanic Niño Index, [https://origin.cpc.ncep.noaa.gov/products/analysis_monitoring/ensostuff/ONI_v5.php];NOAA interpolated outgoing longwave radiation, [https://psl.noaa.gov/data/gridded/data.interp_OLR.html]; International Best Track Archive for Climate Stewardship (IBTrACS v04), (https://www.ncdc.noaa.gov/ibtracs/).

References

An SI, Tziperman E, Okumura YM, Li T (2020) ENSO irregularity and asymmetry. El Niño South Oscil Chang Clim 253:153

Battisti DS, Hirst AC (1989) Interannual variability in a tropical atmosphere865 ocean model: influence of the basic state, ocean geometry and nonlinearity. J Atmos Sci 46(12):1687–1712

Bjerknes J (1969) Atmospheric teleconnections from the equatorial Pacific. Mon Weather Rev 97(3):163–172

Camargo SJ, Wheeler MC, Sobel AH (2009) Diagnosis of the MJO modulation of tropical cyclogenesis using an empirical index. J Atmos Sci 66(10):3061–3074

Capotondi A, Wittenberg AT, Newman M, Di Lorenzo E, Yu J-Y, Braconnot P, Cole J, Dewitte B, Giese B, Guilyardi E et al (2015) Understanding ENSO diversity. Bull Am Meteorol Soc 96(6):921–938

Chang P, Zhang L, Saravanan R, Vimont DJ, Chiang JC, Ji L, Seidel H, Tippett MK (2007). Pacific meridional mode and El Niño—Southern oscillation. Geophys Res Lett 34(16)

Chen D, Lian T, Fu C, Cane MA, Tang Y, Murtugudde R, Song X, Wu Q, Zhou L (2015) Strong influence of westerly wind bursts on El Niño diversity. Nat Geosci 8(5):339

Chiodi AM, Harrison DE, Vecchi GA (2014) Subseasonal atmospheric variability and El Niño waveguide warming: observed effects of the Madden–Julian oscillation and westerly wind events. J Clim 27(10):3619–3642

Chu P-S (1988) Extratropical forcing and the burst of equatorial westerlies in the western Pacific: A synoptic study. J Meteorol Soc Jpn Ser II 66(4), 549–564

Dee DP, Uppala SM, Simmons A, Berrisford P, Poli P, Kobayashi S, Andrae U, Balmaseda M, Balsamo G, Bauer DP et al (2011) The ERA-Interim reanalysis: configuration and performance of the data assimilation system. Q J R Meteorol Soc 137(656):553–597

Eisenman I, Yu L, Tziperman E (2005) Westerly wind bursts: ENSO's tail rather than the dog? J Clim 18(24):5224–5238

Fedorov AV (2002) The response of the coupled tropical ocean-atmosphere to westerly wind bursts. Q J R Meteorol Soc 128(579):1–23

Fedorov AV, Brown JN (2009). Equatorial waves. Encycl Ocean Sci 3679–3695

Fedorov A, Harper S, Philander S, Winter B, Wittenberg A (2003) How predictable is El Niño? Bull Am Meteorol Soc 84(7):911–920

Fedorov AV, Hu S, Lengaigne M, Guilyardi E (2015) The impact of westerly wind bursts and ocean initial state on the development, and diversity of El Niño events. Clim Dyn 44(5–6):1381–1401

Fedorov AV, Hu S, Wittenberg AT, Levine AF, Deser C (2020) ENSO low-frequency modulation and mean state interactions. El Niño South Oscil Chang Clim 253:173

Feng J, Lian T (2018) Assessing the relationship between MJO and equatorial Pacific WWBs in observations and CMIP5 models. J Clim 31(16):6393–6410

Gebbie G, Tziperman E (2009) Predictability of SST-modulated westerly wind bursts. J Clim 22(14):3894–3909

Gebbie G, Eisenman I, Wittenberg A, Tziperman E (2007) Modulation of westerly wind bursts by sea surface temperature: a semistochastic feedback for ENSO. J Atmos Sci 64(9):3281–3295

Gill AE (1980) Some simple solutions for heat-induced tropical circulation. Q J R Meteorol Soc 106(449):447–462

Guilyardi E, Wittenberg A, Fedorov A, Collins M, Wang C, Capotondi A, Stockdale T (2009) Understanding El Niño in ocean–atmosphere general circulation models: progress and challenges. Bull Am Meteor Soc 90(3):325–340

Guilyardi E, Cai W, Collins M, Fedorov A, Jin F-F, Kumar A, Sun D-Z, Wittenberg A (2012) New strategies for evaluating ENSO processes in climate models. Bull Am Meteor Soc 93(2):235–238

Harrison D, Giese BS (1991) Episodes of surface westerly winds as observed from islands in the western tropical pacific. J Geophys Res Oceans 96(S01):3221–3237

Harrison D, Vecchi GA (1997) Westerly wind events in the tropical Pacific, 1986–95. J Clim 10(12):3131–3156

Hartten LM (1996) Synoptic settings of westerly wind bursts. J Geophys Res Atmos 101(D12):16997–17019

Hastings PA (1990) Southern oscillation influences on tropical cyclone activity in the Australian/south-west Pacific region. Int J Climatol 10(3):291–298

Hendon HH, Zhang C, Glick JD (1999) Interannual variation of the Madden–Julian oscillation during austral summer. J Clim 12(8):2538–2550

Hendon HH, Wheeler MC, Zhang C (2007) Seasonal dependence of the MJO931 ENSO relationship. J Clim 20(3):531–543

Hirst AC (1986) Unstable and damped equatorial modes in simple coupled ocean atmosphere models. J Atmos Sci 43(6):606–632

Hu S, Fedorov AV (2016) Exceptionally strong easterly wind burst stalling El Niño of 2014. Proc Natl Acad Sci 113(8):2005–2010

Hu S, Fedorov AV (2017) The extreme El Niño of 2015–2016: the role of westerly and easterly wind bursts, and preconditioning by the failed 2014 event. Clim Dyn 1–19

Hu S, Fedorov AV, Lengaigne M, Guilyardi E (2014) The impact of westerly wind bursts on the diversity and predictability of El Niño events: an ocean energetics perspective. Geophys Res Lett 41(13):4654–4663

Huang B, Thorne PW, Banzon VF, Boyer T, Chepurin G, Lawrimore JH, Menne MJ, Smith TM, Vose RS, Zhang H-M (2017) Extended reconstructed sea surface temperature, version 5 (ERSSTv5): upgrades, validations, and intercomparisons. J Clim 30(20):8179–8205

Iskandar I, Lestari D, Utari P, Sari Q, Setiabudidaya D, Mardiansyah W et al (2018). How strong was the 2015/2016 El Niño event? J Phys Conf Ser 1011:012030. IOP Publishing

Jin F-F, Kim ST, Bejarano L (2006) A coupled-stability index for ENSO. Geophys Res Lett 33(23)

Kessler WS (2001) EOF representations of the Madden–Julian oscillation and its connection with ENSO. J Clim 14(13):3055–3061

Kug J-S, Jin F-F, Sooraj K, Kang I-S (2008). State-dependent atmospheric noise associated with ENSO. Geophys Res Lett 35(5)

Lander MA (1994) An exploratory analysis 957 of the relationship between tropical storm formation in the western north pacific and ENSO. Mon Weather Rev 122(4):636–651

Lengaigne M, Vecchi GA (2010) Contrasting the termination of moderate and extreme El Niño events in coupled general circulation models. Clim Dyn 35:299–313

Lengaigne M, Boulanger J-P, Menkes C, Masson S, Madec G, Delecluse P (2002). Ocean response to the March 1997 westerly wind event. J Geophys Res Oceans 107(C12), SRF–16

Lengaigne M, Boulanger J-P, Menkes C, Madec G, Delecluse P, Guilyardi E, Slingo J (2003) The March 1997 westerly wind event and the onset of the 1997/98 El Niño: understanding the role of the atmospheric response. J Clim 16(20):3330–3343

Levine AF, Jin FF (2017) A simple approach to quantifying the noise-ENSO interaction. part i: Deducing the state-dependency of the wind stress forcing using monthly mean data. Clim Dyn 48(1–2), 1–18

Levine A, Jin FF, McPhaden MJ (2016) Extreme noise-extreme El Niño: How state-dependent noise forcing creates El Niño-La Niña asymmetry. J Clim 29(15):5483–5499

Lian T, Chen D, Tang Y, Liu X, Feng J, Zhou L (2018) Linkage between westerly wind bursts and tropical cyclones. Geophys Res Lett 45(20):11–431

Liang Y, Fedorov AV, Haertel P (2020). Intensification of westerly wind bursts caused by the coupling of the Madden–Julian Oscillation to SST during El Niño onset and development. Geophys Res Lett (accepted)

Liebmann B, Smith CA (1996) Description 982 of a complete (interpolated) outgoing longwave radiation dataset. Bull Am Meteorol Soc 77(6):1275–1277

Liebmann B, Hendon HH, Glick JD (1994) The relationship between tropical cyclones of the western Pacific and Indian Oceans and the Madden-Julian oscillation. J Meteorol Soc Jpn Ser II 72(3):401–412

Madden RA, Julian PR (1972) Description of global-scale circulation cells in the tropics with a 40–50 day period. J Atmos Sci 29(6):1109–1123

Matsuno T (1966) Quasi-geostrophic motions in the equatorial area. J Meteorol Soc Jpn. Ser. II 44 (1), 25–43.

McPhaden MJ (1999) Genesis and evolution of the 1997–98 El Niño. Science 283(5404):950–954

McPhaden MJ (2003) Tropical Pacific Ocean heat content variations and ENSO persis994 tence barriers. Geophys Res Lett 30(9)

McPhaden MJ (2004) Evolution of the 2002/03 El Niño. Bull Am Meteorol Soc 85(5):677–696

McPhaden MJ, Santoso AWC (2020) El Niño southern oscillation in a changing climat.e American Geophysical Union. In press

McPhaden MJ, Yu X (1999) Equatorial waves and the 1997–98 El Niño. Geophys Res Lett 26(19):2961–2964

McPhaden MJ, Zebiak SE, Glantz MH (2006a) ENSO as an integrating concept in earth science. Science 314(5806):1740–1745

McPhaden MJ, Zhang X, Hendon H, Wheeler MC (2006). Large scale dynamics and MJO forcing of ENSO variability. Geophys Res Lett 33 (16).

Neelin JD, Jin F-F (1993) Modes of interannual tropical ocean-atmosphere interaction—a unified view. part ii: analytical results in the weak-coupling limit. J Atmos Sci 50(21):3504–3522

Neelin JD, Jin F-F, Syu H-H (2000) Variations 1006 in ENSO phase locking. J Clim 13(14):2570–2590

Puy M, Vialard J, Lengaigne M, Guilyardi E (2016) Modulation of equatorial Pacific westerly/easterly wind events by the Madden–Julian oscillation and convectively-coupled Rossby waves. Clim Dyn 46(7–8):2155–2178

Puy M, Vialard J, Lengaigne M, Guilyardi E, DiNezio PN, Voldoire A, Balmaseda M, Madec G, Menkes C, Mcphaden MJ (2017). Influence of westerly wind events stochasticity on El Niño amplitude: the case of 2014 vs. 2015. Clim Dyn 1–20

Rasmusson EM, Carpenter TH (1982) Variations in tropical sea surface temperature and surface wind fields associated with the Southern Oscillation/El Niño. Mon Weather Rev 110(5):354–384

Revell CG, Goulter SW (1986) South pacific tropical cyclones and the southern oscillation. Mon Weather Rev 114(6):1138–1145

Roundy PE, Kravitz JR (2009) The association of the evolution of intraseasonal oscillations to ENSO phase. J Clim 22(2):381–395

Rui H, Wang B (1990) Development characteristics and dynamic structure oftropical intraseasonal convection anomalies. J Atmos Sci 47(3):357–379

Seiki A, Takayabu YN (2007) Westerly wind bursts and their relationship with intraseasonal variations and ENSO. part ii: energetics over the western and central Pacific. Mon Weather Rev 135(10):3346–3361

Seiki A, Takayabu YN (2007) Westerly wind bursts and their relationship with intraseasonal variations and ENSO. part i: Statistics. Mon Weather Rev 135(10):3325–3345

Seiki A, Takayabu YN, Hasegawa T, Yoneyama K (2018) Lack of westerly wind bursts in unmaterialized El Niño years. J Clim 31(2):593–612

Slingo J, Rowell D, Sperber K, Nortley F (1999) On the predictability of the interannual behaviour of the Madden–Julian oscillation and its relationship with El Niño. Q J R Meteorol Soc 125(554):583–609

Sobel AH, Maloney ED (2000) Effect of ENSO and the MJO on western North Pacific tropical cyclones. Geophys Res Lett 27(12):1739–1742

Thual S, Majda AJ, Chen N, Stechmann SN (2016) Simple stochastic model for El Niño with westerly wind bursts. Proc Natl Acad Sci 113(37):10245–10250

Timmermann A, An S-I, Kug J-S, Jin F-F, Cai W, Capotondi A, Cobb K, Lengaigne M, McPhaden MJ, Stuecker MF et al (2018) El Niño–Southern Oscillation complexity. Nature 559(7715):535

Torrence C, Webster PJ (1998) The annual cycle of persistence in the El Niño/Southern Oscillation. Q J R Meteorol Soc 124(550):1985–2004

Tziperman E, Yu L (2007) Quantifying the dependence of westerly wind bursts on the large-scale tropical Pacific SST. J Clim 20(12):2760–2768

Vecchi GA, Harrison D (2000) Tropical Pacific sea surface temperature anomalies, El Niño, and equatorial westerly wind events. J Clim 13(11):1814–1830

Vincent EM, Lengaigne M, Menkes CE, Jourdain NC, Marchesiello P, Madec G (2011) Interannual variability of the south Pacific convergence zone and implications for tropical cyclone genesis. Clim Dyn 36(9–10):1881–1896

Wheeler MC, Hendon HH (2004) An all-season real-time multivariate MJO index: development of an index for monitoring and prediction. Mon Weather Rev 132(8):1917–1932

Wheeler M, Kiladis GN (1999) Convectively coupled equatorial waves: analysis of clouds and temperature in the wavenumber-frequency domain. J Atmos Sci 56(3):374–399

Wu X, Okumura YM, DiNezio PN (2019) What controls the duration of El Niño and La Niña events? J Clim 32(18):5941–5965

Yu S, Fedorov AV (2020) The role of westerly wind bursts during different seasons versus ocean heat recharge in the development of extreme El Niño in climate models. Geophys Res Lett 47:e20200GL88381

Zebiak SE, Cane MA (1987) A model El Niño-Southern oscillation. Mon Weather Rev 115(10):2262–2278

Zhang C (2005) Madden–Julian oscillation. Reviews of Geophysics 43 (2)

Zhao B, Fedorov A (2020) The effects of background zonal and meridional winds on ENSO in a coupled GCM. J Clim 33:2075–2091